

Edge-Selector Model Applied for Local Search Neighborhood for Solving Vehicle Routing Problems

Bachtiar Herdianto¹, Romain Billot¹, Flavien Lucas², Marc Sevaux³, and Daniele Vigo⁴

¹*IMT Atlantique, Lab-STICC (UMR 6285, CNRS), Brest, France*

²*IMT Nord Europe, CERI Systèmes Numériques, Douai, France*

³*Université Bretagne Sud, Lab-STICC (UMR 6285, CNRS), Lorient, France*

⁴*DEI "G. Marconi", University of Bologna, Bologna, Italy*

bachtiar.herdianto@imt-atlantique.fr^{*1}

romain.billot@imt-atlantique.fr¹

flavien.lucas@imt-nord-europe.fr²

marc.sevaux@univ-ubs.fr³

daniele.vigo@unibo.it⁴

Abstract

This research proposes a hybrid Machine Learning and metaheuristic mechanism that is designed to solve Vehicle Routing Problems (VRPs). The main of our method is an edge solution selector model, which classifies solution edges to identify prohibited moves during the local search, hence guiding the search process within metaheuristic baselines. Two learning-based mechanisms are used to develop the edge selector: a simple tabular binary classifier and a Graph Neural Network (GNN). The tabular classifier employs Gradient Boosting Trees and Feedforward Neural Network as the baseline algorithms. Adjustments to the decision threshold are also applied to handle the class imbalance in the problem instance. An alternative mechanism employs the GNN to utilize graph structure for direct solution edge prediction, with the objective of guiding local search by predicting prohibited moves. These hybrid mechanisms are then applied in state-of-the-art metaheuristic baselines. Our method demonstrates both scalability and generalizability, achieving performance improvements across different baseline metaheuristics, various problem sizes and variants, including the Capacitated Vehicle Routing Problem (CVRP) and CVRP with Time Windows (CVRPTW). Experimental evaluations on benchmark datasets up to 30,000 customer nodes, supported by pair-wise statistical analysis, verify the observed improvements.

Keywords— Metaheuristic, Vehicle Routing Problems, Binary Classification, Graph Neural Network

1 Introduction

The Vehicle Routing Problems (VRPs) represent a class of combinatorial problems with many applications (Laporte, 2009). Solving them is challenging due to their \mathcal{NP} -hard nature, necessitating using effective search algorithms (Toth and Vigo, 2014). Among them, the Capacitated Vehicle Routing Problem (CVRP) is one of the most extensively studied (Toth and Vigo, 2014; Altabeab, Mohsen, and Ghallab, 2019; Arnold and Sørensen, 2019; Rezaei et al., 2023). Despite extensive research, the CVRP still presents a significant challenge in academic and industrial applications. (Prins, 2004; Marinakis, 2015; Yang et al., 2025). Recently, there has been increasing interest in leveraging ML to improve optimization algorithms (Kool, Hoof, and Welling, 2019; Kwon et al., 2020; Hottung and Tierney, 2020; Bengio, Lodi, and Prouvost, 2021; Ma et al., 2021; Morabit, Desaulniers, and Lodi,

2021; Xin et al., 2021a; Xin et al., 2021b; Mesa et al., 2025). The integration of ML with optimization algorithms can be categorized into three strategies: (1) end-to-end learning, (2) learning based on problem properties, and (3) learning repeated decisions (Bengio, Lodi, and Prouvost, 2021).

The concept of learning from repeated decisions can be implemented by developing an in-loop ML-assisted optimization algorithm, enabling the baseline optimization algorithm to learn from its own decisions and adjust its behavior accordingly (Bengio, Lodi, and Prouvost, 2021). In this paper, we introduce a hybrid optimization framework combining Machine Learning (ML) with metaheuristics to address VRPs. Our key contribution in this paper is the edge selector that identifies prohibited (tabu) moves during local search. We develop two learning-based mechanisms for the edge selector, that is the tabular binary classifier and GNN. Where for the binary classifier we utilize Gradient Boosting Trees (GBT) and Feedforward Neural Network (FNN) as baseline algorithm, with decision threshold optimization to address class imbalance. We further introduce a graph embedding pipeline that directly predict solution edges via structural pattern recognition. The proposed hybrid framework is integrated into two baseline metaheuristics: Fast Iterated Local Search with Localized Optimization (FILO) and Hybrid Genetic Search (HGS). It demonstrates improved performance across both CVRP and CVRPTW instances without requiring fine-tuning for each problem variant.

1.1 Vehicle Routing Problems (VRPs)

In metaheuristic, local search operators are its important components, where it is proven as effective tool for improving solution. The initial idea of local search is that high-quality solutions to an optimization problem might be found by iteratively improving a solution using local neighborhood modifications (Toth and Vigo, 2014). Meanwhile, the utilization of ML, in particular the end-to-end learning framework by means of neural networks for optimization problems can be traced back to a Hopfield network that used to solve small instances of the Traveling Salesperson Problem (TSP) (Hopfield and Tank, 1985). Tabu learning (Beyer and Ogier, 1991), an extension of Hopfield neural networks, incorporates a dynamic, memory-based penalty term into the network’s energy function, preventing the network from revisiting previously encountered suboptimal solutions in continuous non-convex optimization problems.

Meanwhile, the capability of learning by processing graph data is highly important in combinatorial optimization, as many problems can be formulated as graphs (Bengio, Lodi, and Prouvost, 2021). To this end, subsequent research introduced the graph ConvNets (Bresson and Laurent, 2018) to learn rich representations of graph structures, producing edge probabilities that are then transformed into feasible TSP tours using beam search (Joshi, Laurent, and Bresson, 2019). Building on this idea, the resulting heatmaps can also be leveraged to guide Dynamic Programming (Kool et al., 2022a) or even local neighborhood search operators (Hudson et al., 2022). A further advancement comes from NeuroLKH (Xin et al., 2021b), which combines the graph ConvNet (Joshi, Laurent, and Bresson, 2019) with the LKH (Helsgaun, 2017). In this framework, the graph ConvNet is used to assign edge scores and node penalties, which in turn guide the LKH.

However, scalability and generalizability still need to be further investigated. In particular, prior research often requires fine-tuning every variants of the problem. Additionally, the quality of the solutions still needs improvement, as it remains lower than that achieved by already established methods. The learning repeated decision then falls into two approaches: optimization enhanced by learning and learning enhanced by optimization.

Learning Enhanced by Optimization In the first category, the ML model plays the primary role in refining solutions, while a simple search algorithm supports the process. These methods typically involve ML models that directly construct or guide the solution path. Early examples include NeuRewriter (Chen and Tian, 2019), which used basic local search heuristics and Learn to Improve (L2I) (Lu, Zhang, and Yang, 2020), which uses a reinforcement learning controller to select improvement operators based on solution states. Subsequent research has then focused on controlling the k -opt heuristic. One of the earliest works proposed a deep reinforcement learning to guide 2-opt (Wu et al., 2021), later improved by the Dual-Aspect Collaborative Transformer (DACT) (Ma et al., 2021), which introduced Dual-Aspect Collaborative Attention (DAC-Att) and a cyclic positional encoding method to guide 2-opt. Additionally, an RNN-based policy was proposed to govern 2-opt operations (Costa et al., 2020),

which was later extended to 3-opt (Sui et al., 2021) by incorporating the Feature-wise Linear Modulation Network (FiLM-Net) (Gupta et al., 2020). FiLM-Net modulates current solution features with selected link features as conditioning information to output appropriate reconnection types. However, these neural k -opt solvers are still constrained by small and fixed values of k . Further improvements were made in NeuroLKH (Ma, Cao, and Chee, 2023), which directly utilizes LKH (Helsgaun, 2017) as the baseline solver to improve subproblems guided by GNN-predicted heatmaps, allowing for more flexible k -move improvements.

Nevertheless, while some of these methods demonstrate generalizability, they still require fine-tuning for different problem variants. Moreover, future research is needed to enhance scalability and to demonstrate that the solution quality produced by these mechanisms can match or exceed that of current state-of-the-art solvers.

Optimization Enhanced by Learning In the second category, advanced optimization algorithms play the primary role in refining solutions, with ML models providing auxiliary guidance to enhance decision-making within the search process. A representative example is the *learning-to-delegate* mechanism introduced for large-scale CVRP instances (Li, Yan, and Wu, 2021), which integrates ML with state-of-the-art metaheuristic algorithms such as LKH (Helsgaun, 2017) and HGS (Vidal, 2022) to improve scalability. Their approach uses a Transformer-based model (Kool, Hoof, and Welling, 2019) to select subregions for refinement via subsolvers, in which the metaheuristic algorithms. Extending this direction, DeepACO (Ye et al., 2023) combines ML with Ant Colony Optimization (ACO) (Dorigo, Birattari, and Stutzle, 2006), using GNNs to predict heatmaps to guide the probabilistic search process. This was later advanced by the Generative Flow Ant Colony Sampler (GFACS) (Kim et al., 2025), which used Generative Flow Networks (GFlowNets) (Bengio et al., 2021) to learn a reward-proportional sampling distribution for guiding both ant sampling and pheromone updates.

The GNN (Gori, Monfardini, and Scarselli, 2005; Scarselli et al., 2009) have also been applied to column selection for guiding column generation procedure (Morabit, Desaulniers, and Lodi, 2021), reducing computational time without compromising solution quality. In the domain of hybrid mechanisms aimed at enhancing local search, GNN-GLS (Hudson et al., 2022) leverages a graph ConvNet (Joshi, Laurent, and Bresson, 2019) to predict regret values for each edge in the problem instance, informing Guided Local Search (GLS) (Arnold and Sørensen, 2019) about which edges to penalize. In contrast, NeuroLS (Falkner et al., 2023) employed a k -GNN (Morris et al., 2019) to control the local search procedure directly. Further exploration into learning-based local search includes the Learning to Guide Local Search (L2GLS) framework (Sultana et al., 2024), which employs policy network with attention-based encoding is trained to dynamically select local search operators at each step, based on the current solution state and recent action history. Further, the subsequent research introduces a learning-guided segmentation framework for CVRP that uses global graph-level features via Graph Attention Networks (GAT) (Veličković et al., 2018) to identify stable solution segments (Ouyang et al., 2025). These stable segments are aggregated and fixed, enabling the baseline heuristic to focus subsequent search iterations on the remaining unstable parts of the solution.

Although these hybrid mechanisms show promise and in some cases outperform their respective baselines, much of the existing research lacks rigorous statistical validation to confirm significant improvements. Moreover, while many of these approaches are applicable across a range of routing problems, they typically require training or fine-tuning the ML models for each new problem variant, limiting generalizability.

1.2 Research Questions and Contributions

The mechanism *learning repeated decision* employs an in-loop ML-guided optimization framework, in which a baseline algorithm manages the high-level search process and iteratively invokes a machine learning model to guide lower-level decisions (Bengio, Lodi, and Prouvost, 2021). This structure allows the algorithm to adapt its behavior over time by leveraging accumulated experience.

Although hybrid approaches combining ML and optimization have gained increasing attention (Hottung and Tierney, 2020; Bengio, Lodi, and Prouvost, 2021), generalization remains a significant challenge (Bengio, Lodi, and Prouvost, 2021), particularly in real-world applications where problem distributions can vary substantially. Another key concern is scalability, as hybrid models must be capable of handling large-scale and complex optimization

problems (Bengio, Lodi, and Prouvost, 2021).

Prior studies on VRP solvers indicate that solution-based features are often more effective for guiding optimization algorithms (Arnold and Sörensen, 2019; Lucas, Billot, and Sevaux, 2019). At the same time, recent advances in Graph Neural Networks (GNNs) have demonstrated strong performance in diverse domains (Dwivedi et al., 2023), including their application in routing problems (Joshi, Laurent, and Bresson, 2019; Kool et al., 2022a; Joshi et al., 2022). Building upon these insights, this research is designed to address the following questions:

1. How can an edge selector model be developed to classify solution edges and identify areas with potential improvement accurately?
2. How can we design an effective hybrid mechanism that integrates the learned model to enhance the performance of the metaheuristic baselines?
3. How can we ensure that the hybrid mechanism generalizes sufficiently across different problem variants while avoiding the need for fine-tuning the learning model?

To address these questions, we propose the *edge selector model*, a ML model capable of classifying the edges of a VRP solution. This model aims to dynamically control the neighborhood exploration during local search improvement phase while filtering unnecessary moves by reducing the search space. In summary, our contributions are:

1. The edge selector model that predicts areas of improvement in a VRP solution, filtering non-promising moves within local search neighborhoods.
2. A hybrid mechanism that integrates the proposed edge-solution selector model with metaheuristic baselines to solve the CVRP.
3. A generalized hybrid mechanism by extending the developed for the CVRP for solving the CVRPTW without fine-tuning the baseline ML model.

The remainder of this paper is organized as follows: Section 2 presents the baseline metaheuristics used as baseline for developing our proposed hybrid mechanism. Section 3 details the architecture and components of our proposed hybrid pipeline, while Section 4 explains the generalization principle operated in the proposed hybrid mechanism. Section 5 shows the experimental setup and comparative evaluation of our proposed hybrid mechanism. Finally, Section 6 summarizes our findings.

2 Baseline Metaheuristics

Local search neighborhoods form the important mechanism of metaheuristics (Prodhon and Prins, 2016; Arnold and Sörensen, 2019). Metaheuristics for solving VRPs in general can be categorized into two main classes: *path-based methods* and *population-based methods* (Prodhon and Prins, 2016). Path-based methods employ a simple iterative mechanism during optimization, where local search neighborhoods are applied to progressively improve solution. These methods typically incorporate solution acceptance criteria to balance exploration and exploitation. A representative example is the Fast Iterated Local Search Localized Optimization (FILO) metaheuristic (Accorsi and Vigo, 2021), which consists of a construction phase, followed by an improvement phase involving the optional route minimization and core optimization procedure that applies various local search neighborhoods. Meanwhile, population-based methods maintain and evolve a diverse set of solutions simultaneously. These approaches utilize recombination operators coupled with local search mechanisms to guide the population toward high-quality feasible solutions. The Hybrid Genetic Search (HGS) metaheuristic (Vidal, 2022) represents this category, maintaining both feasible and infeasible solutions in its population while employing local search neighborhoods to drive the optimization process toward feasible good solutions.

Local search neighborhoods Local search provides a simple yet effective procedure for improving solution in combinatorial optimization in which tasks of the type $\min_{x \in X} c(x)$, where X is the set of feasible solutions and c denotes the cost function. The neighborhood $\mathcal{N}_r(x)$ of a solution x is the set of all solutions that can be

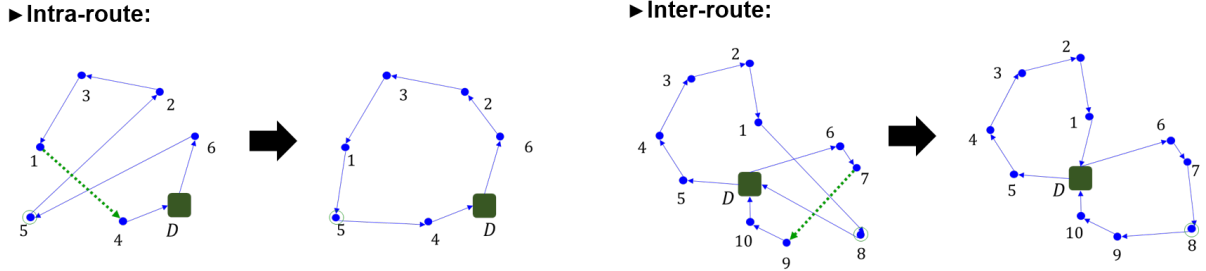


Figure 1: Reallocation involves relocating a node to a new position within the current solution.

obtained by applying any move τ from a predefined set of transformations \mathcal{T} to x , $\mathcal{N}_\tau(x) = \{\tau(x) \mid \tau \in \mathcal{T}\} \subset X$. In the case of the CVRP, the neighborhood $\mathcal{N}_\tau(x)$ is commonly determined relative to a set of moves that can modify the current solution \mathcal{S} . Each move τ corresponds to a minor change that transforms x into a neighboring solution $\tau(x) \in \mathcal{N}_\tau(x)$. Figure 1 illustrates examples of local search moves. The local search operation reallocates a customer node by inserting it at a new position in the current solution. This move can be performed within the same route (intra-move) or between different routes (inter-move).

Tabu search mechanism Tabu Search escapes local optima by keeping a tabu list of recent moves. A move is prohibited if it matches any entry in this list. Further, the concept of an aspiration criterion allows the algorithm to override the tabu status when a move results in a better solution, promoting flexibility in the search process (Glover and Laguna, 1998).

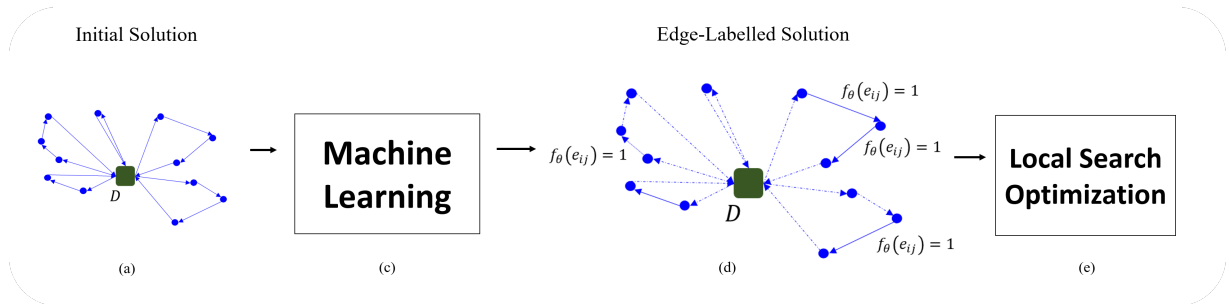


Figure 2: Overview of the proposed hybrid framework.

3 The Edge Solution Selector Model

In the proposed hybrid mechanism, prohibited (tabu) moves are predicted before performing local search. This is accomplished by developing an edge selector model f_θ that assigns binary labels $f_\theta(e_{ij}) \in \{0, 1\}$ for every edge $\forall i, j \in E$ in the graph. By labeling these edges, we can control the behaviour of the local search, aiming to reduce the search space and avoid unnecessary moves. As illustrated in Figure 2, the mechanism begins by constructing the initial solution S_0 in (a) from the problem instance. The proposed edge selector model f_θ is implemented in (b), which predicts labels for all edges in $E(S_0)$ (c). These labels guide the improvement process, where further improvements are achieved via a set of local search operators (d). Moreover, when the metaheuristic baseline employs a multi-start search strategy (Prodhon and Prins, 2016), the process of construction S_0 , prediction, and local search is repeated iteratively until the termination criterion is met.

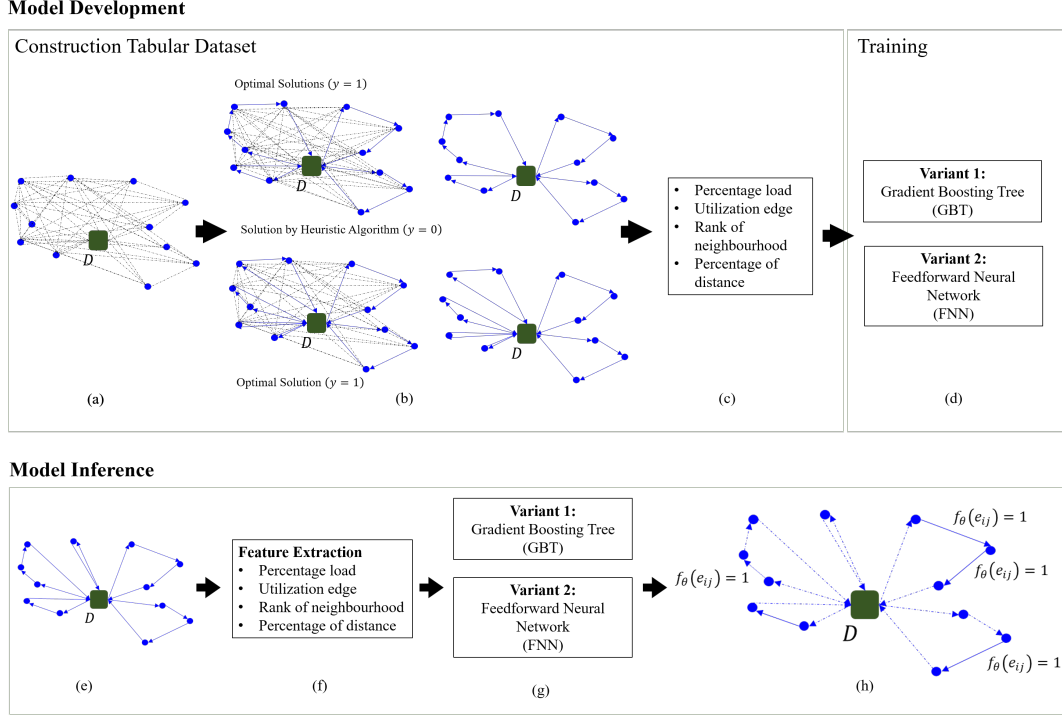


Figure 3: Overview of the hybrid framework using tabular classifiers as the baseline learning model.

3.1 Tabular Binary Classification

In this mechanism, the solution S_0 is transformed into a two-dimensional feature matrix \mathbf{X} . This matrix is constructed using p features that describe the edge structure of S_0 . Each edge in S_0 , denoted as $E(S_0) \subseteq E$, is then labeled by the selector f_θ . The resulting matrix \mathbf{X} has dimensions $|E(S_0)| \times p$, where $|E(S_0)|$ is the number of edges in S_0 and p is the number of features. The selector function f_θ operates as follows:

$$f_\theta : E(S_0) \rightarrow \{0, 1\} \quad (1)$$

As illustrated in Figure 3, the development of the tabular model involves two main stages: constructing the tabular solution-edge dataset for training (a to c), and training the baseline classifier through a supervised learning approach (d). The dataset construction begins by solving 10,000 instances from the XML100 benchmark (Queiroga et al., 2021), which includes both optimal¹ and non-optimal solutions. As shown in subfigure (b), the non-optimal solutions are generated via the Savings (S_{cu}) and Sweep (S_{sweep})² heuristics, as well as the MNS-TS (S_{mns}) (Soto et al., 2017) algorithm. The resulting tabular dataset used to train the classifier baseline consists of pairs of edge features and labels $(x_{(i)}, y_{(i)})$ between customer nodes C , where $x_{(i)}, y_{(i)} \in \mathcal{D}$ and $i \in \mathbb{N}$. Further details about the features used in the tabular mechanism are provided in subfigure (c) and described in A.1. As depicted in (d), we develop two classifier variants of the selector model f_θ for the tabular mechanism: Gradient Boosting Tree (GBT) and Feedforward Neural Network (FFN). Moreover, designing the tabular learning architecture f_θ involves defining the classifier structure and addressing class imbalance, which arises from the disparity between the number of edges in the solution and the total number of possible edge combinations. To ensure both models output a probability score indicating the likelihood of each edge belonging to the optimal solution, a sigmoid activation function $\sigma(z) = 1/(1+e^{-z})$ is applied at the final layer. Lastly, as illustrated in Figure 3 (e to h), during inference with the hybrid mechanism using the tabular baseline, the process begins by extracting an initial solution, as shown in subfigure (e). Edge-solution features are computed in (f) and then passed to the classifier in (g), which produces an edge-labeled solution in (h). This labeled solution is subsequently used to guide the improvement

¹Provided by Queiroga et al. (2021)

²Implemented using the solver by Groër, Golden, and Wasil (2010): <https://github.com/coin-or/VRPH>

phase, where further enhancements are achieved using a set of local search operators.

Gradient Boosting Tree In the first variant, the tabular variant of the selector f_θ is implemented using the GBT. Given an input vector $\mathbf{X} \in \mathbb{R}^p$, the GBT model with M estimators performs binary classification. Let $h_m(\mathbf{X})$ be the prediction from the m -th estimator, the final prediction is:

$$f(\mathbf{X}) = \sigma(F_M(\mathbf{X})) = \sigma\left(\sum_{m=1}^M \gamma_m h_m(\mathbf{X})\right) \quad (2)$$

where γ_m is its learning rate and $\sigma(\cdot)$ is the sigmoid activation function, mapping outputs to the range $(0, 1)$.

Feedforward Neural Network In the second variant, we implement the tabular variant of the selector f_θ using the FNN as a baseline classifier. Given an input vector $x \in \mathbb{R}^p$, the FNN consists of L layers for binary classification. Let M_l denote the number of neurons in the l -th layer, with $M_0 = p$, $M_L = 1$, and $M_l = d_l$ for $0 < l < L$. The weight matrix and bias vector for layer l are denoted as \mathbf{W}_l and \mathbf{b}_l , respectively. The selector’s prediction is given by:

$$f(\mathbf{X}) = \sigma\left(\mathbf{W}_L^\top \dots \text{ReLU}\left(\mathbf{W}_1^\top x + \mathbf{b}_1\right) \dots + \mathbf{b}_L\right) \quad (3)$$

Each hidden layer uses the ReLU (Rectified Linear Unit) as the activation function, $\text{ReLU}(z) = \max(0, z)$, and the last layer applies the sigmoid function $\sigma(\cdot)$.

Thresholding under class imbalance As mentioned earlier, the main challenge in this mechanism is handling class imbalance, as the number of solution edges is much smaller than the total possible edges. To address this in tabular binary classification, we explore two thresholding strategies. The sigmoid output σ from the baseline algorithms require a threshold t , which plays a critical role in imbalanced settings (Narasimhan, Vaish, and Agarwal, 2014; Singh and Khim, 2022). For the selector f_θ , the goal is to minimize false positives while accurately identifying true prohibited moves. While the default threshold is $t = 0.5$, in this research, we apply a deterministic rule:

$$\hat{f}(x) = \begin{cases} 1 & \text{if } f(x) > t \\ 0 & \text{otherwise} \end{cases} \quad \text{with } 0 < t < 1 \quad (4)$$

Alternatively, we also apply stochastic threshold decision rule to account robustness near the decision boundary.

$$\hat{f}(x) = \begin{cases} 1 & (f(x) > t + \epsilon) \vee (\text{abs}(f(x) - t) < \epsilon \wedge p > \mathcal{R}) \\ 0 & \text{otherwise} \end{cases} \quad (5)$$

where ϵ is a small positive constant used as a tolerance for numerical comparison and $\mathcal{R} \sim \mathcal{U}(0, 1)$. Both methods are applied to improve the performance of the selector f_θ under class imbalance.

3.2 Graph Neural Networks

Recent GNN-based hybrid optimization solvers incorporated GNNs with heuristic search to approximate solutions for graph-structured problems (Joshi, Laurent, and Bresson, 2019; Joshi et al., 2022; Kool et al., 2022a; Dwivedi et al., 2023). Subsequently, to further enhance the performance of the selector f_θ , we explore the use of GNNs as a baseline learning model. In this research, we build upon these existing methods by leveraging edge prediction capabilities in GNNs to guide the search process, in particular, to identify prohibited moves during local search neighborhood exploration. Similar to the tabular baseline, the development of the graph-based model, as illustrated in Figure 4, involves two main stages: (1) constructing the training dataset (a), and (2) training the model (b to d). The dataset, consisting of CVRP instances and their corresponding solutions, is divided into small-scale and large-scale instances. The baseline graph learning model is then trained using this dataset through a supervised learning approach. During inference, the hybrid mechanism begins by generating an initial solution S_0 (e), which is then passed to the edge selector model f_θ (f). The selector then predicts the likelihood of each edge in S_0 being part of a high-quality solution. This results in an edge-labeled solution (h), which is then used to guide the improvement phase. Here, a set of local search operators is applied in this phase to refine the solution further.

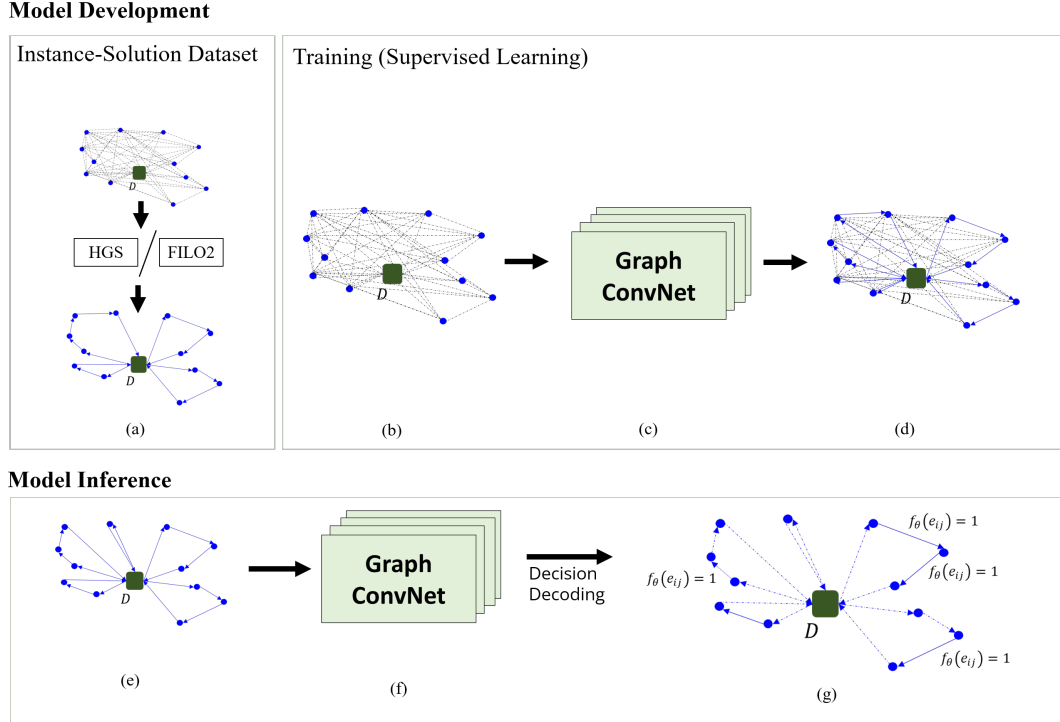


Figure 4: Overview of the hybrid framework with Graph ConvNet as the baseline learning model.

In Figure 4, the initial solution S_0 is used as input to the selector f_θ . The S_0 can be represented a sparse graph, which serves as the basis for predicting the likelihood that its edges belong to a high-quality solution. We extend the probabilistic output of the selector f_θ by applying a deterministic threshold t , as defined in Equation (4), to determine whether an edge should be prohibited from being involved in local search moves.

Graph embedding We extend the graph Convolutional Network (ConvNet) architecture (Joshi, Laurent, and Bresson, 2019; Kool et al., 2022a) to develop a hybrid node-destroyer model that guides the removal of customer nodes during local search. Unlike prior works that primarily employ graph ConvNets to construct solutions from scratch (Joshi, Laurent, and Bresson, 2019; Kool et al., 2022a; Joshi et al., 2022; Dwivedi et al., 2023), our approach leverages the model to evaluate and select components within an existing solution. The graph ConvNet incorporates anisotropic message passing with edge gating, enabling the iterative update of both node and edge representations across network layers. Each input node feature is represented as a three-dimensional vector $x_i \in [0, 1]^3$, encoding the node’s coordinates and its demand utilization q/Q .

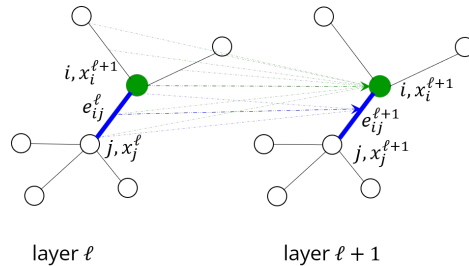


Figure 5: Representation message passing in graph ConvNet.

The edge features, corresponding to the rounded Euclidean distances d_{ij} , are embedded into an $h/2$ -dimensional vector space. Let x_i^ℓ and e_{ij}^ℓ denote the node and edge feature vectors at layer ℓ , respectively. The node update

rule is defined as:

$$x_i^{\ell+1} = x_i^\ell + \text{ReLU} \left(\text{BN} \left(W_1^\ell x_i^\ell + \sum_{j \sim i} \eta_{ij}^\ell \odot W_2^\ell x_j^\ell \right) \right) \quad (6)$$

where η_{ij}^ℓ is the attention map, computed as:

$$\eta_{ij}^\ell = \frac{\sigma(e_{ij}^\ell)}{\sum_{j' \sim i} \sigma(e_{ij'}^\ell) + \epsilon} \quad (7)$$

with $\sigma(\cdot)$ denoting the sigmoid activation and ϵ a small constant for numerical stability. The edge features are updated using the following rule:

$$e_{ij}^{\ell+1} = e_{ij}^\ell + \text{ReLU} \left(\text{BN} \left(W_3^\ell e_{ij}^\ell + W_4^\ell x_i^\ell + W_5^\ell x_j^\ell \right) \right) \quad (8)$$

Here, $W \in \mathbb{R}^{h \times h}$ denotes a learnable weight matrix. The function BN refers to Batch Normalization, which normalizes activations within each mini-batch. As illustrated in Figure 5, the model stacks multiple layers to refine node and edge embeddings iteratively. The green and blue arrows in the figure indicate the information flow between nodes and edges, enabling the model to learn structural representations from the input graph to estimate the likelihood that each edge belongs to a high-quality solution.

Curriculum learning We initially train our GNN-based selector f_θ on the CVRP instances and solution dataset of size $N = 100$ (Kool et al., 2022a). Hence, to improve the scalability and generalization of the baseline model to handling larger problem sizes, we leverage a curriculum learning strategy, where the model is progressively trained on instances of increasing complexity (Bengio et al., 2009). In particular, the selector f_θ is further trained on larger instance-solution dataset, with size $N = 1,000$. This dataset is generated using the $\mathbb{X}\text{ML}100$ instance generator³ (Queiroga et al., 2021). A total of 100,000 instances are generated and then solved by using the FILO2 (Accorsi and Vigo, 2024)⁴, which provides high-quality labels for further training the model. This strategy enables the selector f_θ to scale on larger CVRP instances.

Model inference While the training phase utilizes the full graph for the CVRP instances with $N = 100$, and a sparse graph with $k = 25$ nearest neighbors for $N = 1,000$, the inference phase adopts a different approach. Specifically, during inference, edge evaluation is restricted to those forming the initial solution $E(S_0) \subseteq E$, generated by the baseline metaheuristic. In other words, the model operates on a sparse graph, derived from S_0 , as illustrated in Figure 6. The performances of the selector f_θ during model inference can be measured using the precision score. The goal of f_θ is to maximize the number of edges correctly classified as prohibited moves that are indeed part of the high quality (groundtruth) solution, while minimizing the number of edges wrongly predicted as prohibited that do not belong to the groundtruth. Let TP (*True Positive*) be defined as $\text{TP} := \mathbb{P}(\hat{f}(\mathbf{x}) = 1 \wedge y = 1)$, and let FP (*False Positive*) be defined as $\text{FP} := \mathbb{P}(\hat{f}(\mathbf{x}) = 1 \wedge y = 0)$. This aligns with the binary classification setting, in which maximizing true positives and minimizing false positives. Thus, the precision score is computed as:

$$\text{precision} := \mathbb{P}(y = 1 \mid \hat{f}(\mathbf{x}) = 1) = \frac{\mathbb{P}(\hat{f}(\mathbf{x}) = 1 \wedge y = 1)}{\mathbb{P}(\hat{f}(\mathbf{x}) = 1)} = \frac{\text{TP}}{\text{TP} + \text{FP}} \quad (9)$$

As illustrated in Figure 6, for an instance with 22 customer nodes, the initial solution S_0 is shown in subfigure (a). The selector predicted 26 prohibited edges, as depicted in subfigure (b). When comparing subfigure (b) to the groundtruth in subfigure (c), we observe that 22 of these edges are TP, while the remaining 4 are FP, resulting in a precision score of 0.8461. This demonstrates that the predictions made by the selector f_θ closely align with the ground truth structure.

³Available at <http://vrp.galgos.inf.puc-rio.br/index.php/en/>

⁴These instances and solutions are available at <https://github.com/bachtiarherdianto/MH-Edge-Selector>

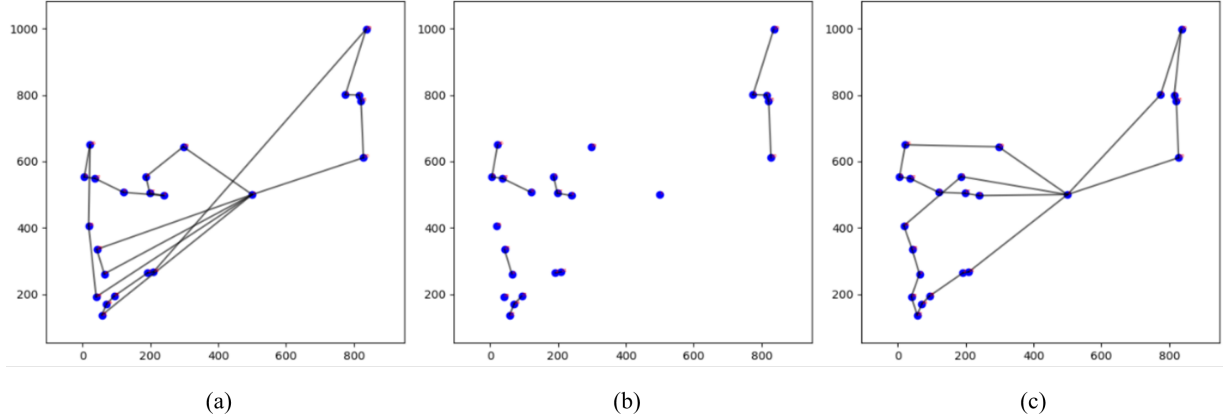


Figure 6: Overview model inference from a CVRP instance with $n = 22$.

Solving very large scale problems Utilizing sparse graphs helps speed up the training and inference phases without a major loss in prediction quality (Kool et al., 2022a). For instances larger than 1,000 customer nodes, the size of the full graph results in significant computational overhead. To manage this, inference is limited to the subset of edges that define the initial solution S_0 . Accordingly, only the 1,000 nearest nodes to the depot c_0 are used by the selector f_θ in very large-scale problem instances. Experimental analysis during model development confirms that this scalable strategy lowers runtime computation without sacrificing prediction quality.

4 Generalization

While previous research has explored generalization in constructive algorithms within end-to-end learning framework (Hottung and Tierney, 2020; Jiang et al., 2023; Li et al., 2023), our study presents a framework that generalizes through iterative learning repeated decision mechanism. Given that a feasible VRP solution consists of a set of routes R , each starting and ending at the depot c_0 , where every route r_k satisfies the capacity constraint $q(r_k) \leq Q$ and each customer is visited exactly once, we investigate two aspects of generalization. The first aspect is applying the selector f_θ to different VRP variants, such as CVRP and CVRPTW. And the last one is integrating the selector f_θ with different baseline metaheuristics. Proposition 4.1 presents the generalization capability of the proposed hybrid mechanism, specifically in solving VRPs.

Proposition 4.1. *The selector f_θ , designed to fix (prohibited) specific edges rather than generate complete solutions, can generalize beyond the CVRP to other VRP variants.*

Proof. Let \mathcal{F} denote the set of fixed (prohibited) edges in solution S , and E the set of remaining (adjustable) edges, such that $\mathcal{F} \cup E = S$. Local search operators, when applied under the feasibility constraints of a problem, produce a modified set E' . Since both \mathcal{F} and E' satisfy the constraints of the VRPs, the new solution $S' = \mathcal{F} \cup E'$ remains feasible. \square

5 Experiment and Analysis

We implemented the baseline solver in C++ and selector f_θ in Python⁵. The experiments were conducted on a 64-bit Debian GNU/Linux 12 machine with 16 virtual AMD cores, 62 GB RAM, and an NVIDIA L40 GPU. Considering the pseudo-random aspect (Matsumoto and Nishimura, 1998), each experiment involved five runs, with the random seed was defined as the run counter minus one. Throughout the experimentation, we refer to the following:

⁵Available at <https://github.com/bachtiarherdianto/MH-Edge-Selector>

- BKS: the total cost value of the best-known solutions. All the information related to the instances and best-known solutions are available at <http://vrp.galgos.inf.puc-rio.br/index.php/en/>.
- Gap: represents the relative deviation of a solution from the optimal solution, or from the best-known solution (BKS) if the optimal remains unknown. It is given by:

$$\text{Gap} = \frac{\text{Obtained Solution} - \text{BKS}}{\text{BKS}} \times 100\% \quad (10)$$

Experiment setup The selector f_θ is developed using two learning-based mechanisms: the tabular binary classifier and a graph learning, as summarized in Table 1. For the tabular models, the baseline GBT requires only around 8 minutes for training, while the FNN takes approximately 20 hours. However, both training processes are relatively short and can be performed without GPU acceleration, as the learning architecture for the tabular models is significantly simpler compared to the graph-based model. Subsequently, training the baseline graph-based model is more heavy. It was conducted supported with NVIDIA L40 GPU. During evaluation on the validation and test sets, the adjacency matrix, which represents the probabilities of all edges in the initial solution obtained from the graph ConvNet, is converted into binary decisions.

Using high-quality solutions as ground-truth labels, precision is computed as described in Section 3.2. The selector model f_θ was first trained on CVRP instances with $N = 100$, using labels generated from high-quality HGS solutions Kool et al., 2022a. This initial training phase took approximately 1.6 hours and used about 2 GB of GPU memory. To adapt f_θ to more complex problems with $N = 1,000$, we employed a curriculum learning strategy by further training the model on larger instances. This curriculum learning phase consumed 42.9 GB of GPU memory and lasted around 7.5 hours. The curriculum learning approach improved the model’s effectiveness on large-scale instances.

Table 1: Various Hybrid Mechanisms with Baseline FILO2.

Hybrid Mechanism	Learning Model			Binary Thresholding	
	Tabular		Graph	Deterministic	Stochastic
	GBT	FNN	ConvNet		
FILO2- α	✓			✓	
FILO2- β	✓				✓
FILO2- γ		✓		✓	
FILO2- δ		✓			✓
FILO2- μ			✓	✓	

For the experiment, as summarized in Table 1, there are five hybrid variants of FILO2 in total. Variants α , β , γ , and δ employ tabular binary classifiers, while variant μ leverages deep graph learning. The tabular classifier employs the Gradient Boosted Trees (GBT) and the Feedforward Neural Network (FNN) as baseline algorithms. Given Equation (2) for GBT and Equation (3) for FNN, we set $\mathbb{M} = 100$ for GBT, and configure the FNN with $\mathbb{L} = 2$ hidden layers, each consisting of 256 neurons. Threshold adjustments are applied to address class imbalance, which align with Equation (4) and Equation (5). In FILO2, deterministic thresholds are set at $t = 0.8$ for both algorithms. Under stochastic thresholding, we use $t = 0.8$ with acceptance probabilities $p = 0.9$ for GBT and $p = 0.75$ for FNN. The graph model extend the graph *Convolutional Network* (ConvNet) architecture (Joshi, Laurent, and Bresson, 2019; Kool et al., 2022a; Dwivedi et al., 2023) for direct binary solution’s edge prediction. For graph model in FILO2, $t = 0.8$ is used for \mathbb{X} instances and $t = 0.75$ for \mathbb{B} instances. We also apply the tabu aspiration mechanism (Glover, 1997) using a randomized threshold p_Θ , allowing prohibited edges to performs move when $\mathcal{R} \sim \mathcal{U}(0, 1)$ exceeds p_Θ . For FILO2, we set $p_\Theta = 0.8$ for tabular models, and $p_\Theta = 0.6$ and 0.8 for graph model on \mathbb{X} and \mathbb{B} respectively.

Statistical analysis This analysis is conducted to assess the significant effect of the proposed mechanism. We performed the non-parametric one-tailed Wilcoxon signed-rank test (Demšar, 2006; Arnold et al., 2021; Accorsi, Lodi, and Vigo, 2022; Zárate-Aranda and Ortiz-Bayliss, 2025) to compare the baseline and proposed hybrid mechanism, with Hypotheses H_0 and H_1 formulated as follows:

Hypothesis H_0 . *There is no statistically significant difference*

Hypothesis H_1 . *There is a statistically significant difference*

In this research, we set $\alpha = 0.05$ (Arnold et al., 2021; Zárate-Aranda and Ortiz-Bayliss, 2025). If the p -value $> \alpha$, we fail to reject H_0 , indicating that the average results of the two methods are not statistically different. If the p -value $\leq \alpha$, we reject H_0 , in which indicating that the average results of the proposed hybrid mechanism are statistically better compared with the baseline.

Algorithm 1 The Edge-Selector f_θ applied in FILO2.

Input: Problem instance: P

Output: Solution: S

```

1: procedure HYBRID-FILO2( $P$ )
2:    $S_0 \leftarrow$  CONSTRUCTINITIALSOLUTION( $P$ )
3:    $\mathcal{X} \leftarrow$  FEATUREEXTRACTION( $S_0$ )
4:    $S' \leftarrow f_\theta(\mathcal{X})$  ▷ edge-labeled solution
5:    $k \leftarrow$  GREEDYROUTEESTIMATE( $P$ )
6:   if Route( $S'$ )  $> k$  then
7:      $S' \leftarrow$  ROUTEMIN( $S'$ )
8:   end if
9:    $S \leftarrow$  COREOPTIMIZATION( $S'$ )
10: end procedure

```

5.1 Experiment with FILO2

The pseudocode for the proposed hybrid edge selector mechanism integrated with the baseline FILO2 algorithm (Accorsi and Vigo, 2024) is shown in Algorithm 1. FILO2 begins with a construction phase that builds an initial feasible solution using a restricted version of the savings algorithm (Clarke and Wright, 1964; Arnold, Gendreau, and Sörensen, 2019). This is followed by an improvement phase, which may first attempt to reduce the number of routes if they are considered excessive. Subsequently, a core optimization process iteratively refines the solution through a localized optimization scheme. In our approach, the selector is applied after the initial solution S_0 is constructed. We embed S_0 and label each edge in the solution using the selector model f_θ . These labels then guide the subsequent local search optimization phase as the algorithm refines S_0 .

Table 2: Summary of the average gap to the BKS over 5 runs on FILO2 (time in seconds).

Problem Size	Baseline		Proposed Hybrid Mechanisms									
	FILO2		FILO2- α		FILO2- β		FILO2- γ		FILO2- δ		FILO2- μ	
	Gap (%)	Time	Gap (%)	Time	Gap (%)	Time	Gap (%)	Time	Gap (%)	Time	Gap (%)	Time
× Instances												
101 - 200	0.138	91.26	0.138	68.36	0.138	69.66	0.131	68.00	0.143	67.32	0.114	117.73
204 - 491	0.310	88.82	0.311	69.49	0.310	70.89	0.335	70.24	0.340	72.07	0.350	114.58
502 - 1001	0.493	87.77	0.492	69.27	0.492	70.70	0.498	69.84	0.501	71.46	0.481	113.22
Average Gap	0.331	89.02	0.331	69.18	0.331	70.56	0.342	69.62	0.348	70.83	0.340	114.84
ℬ Instances												
3k - 7k	0.742	103.55	0.742	98.27	0.742	100.75	0.721	98.50	0.728	100.29	0.686	124.75
10k - 16k	1.262	109.15	1.262	106.02	1.262	110.05	1.274	105.63	1.294	108.50	1.241	144.00
20k - 30k	1.422	123.70	1.406	124.85	1.422	130.74	1.436	124.23	1.501	126.95	1.391	171.05
Average Gap	1.086	112.96	1.083	110.48	1.086	114.36	1.085	110.17	1.109	112.44	1.049	146.58

Computational results To assess the performance of the proposed hybrid mechanism compared with the baseline FILO2, we perform experiments utilizing both \times and \mathbb{B} instances to evaluate its effectiveness and scalability. Table 2 presents a performance comparison between the baseline FILO2 and six variants of the proposed

hybrid learning mechanisms. For the \mathbb{X} instances, the hybrid variants generally maintain or slightly improve the gap compared to the baseline, while significantly reducing computational time, particularly those using a simple tabular architecture. Notably, FILO2- μ , which is based on a GNN architecture, achieves the most significant performance improvement. In the \mathbb{B} instances, the hybrid mechanisms again demonstrate competitive performance, with FILO2- μ consistently outperforming all other variants and the baseline across customer sizes.

Table 3: Average gap to BKS on \mathbb{X} instances under different customer distribution.

Customer Distribution	Baseline	Proposed Hybrid Mechanisms				
	FILO2	FILO2- α	FILO2- β	FILO2- γ	FILO2- δ	FILO2- μ
Random (R)	0.260	0.258	0.258	0.266	0.282	0.260
Clustered (C)	0.377	0.377	0.377	0.380	0.398	0.373
Random-Clustered (RC)	0.337	0.337	0.337	0.352	0.351	0.353

However, this improvement comes with increased computation time, due to the overhead of model inference from the Deep Learning-based architecture. Among the tabular models, variants α and δ show marginal gains, but not to the extent observed with variant μ .

Table 4: Detailed results variant μ in solving \mathbb{B} instances (time in seconds).

Instance	FILO2			FILO2- μ			BKS
	Avg (Gap)	Best (Gap)	Time	Avg (Gap)	Best (Gap)	Time	
Leuven1	193683 (0.433)	193627 (0.404)	90.4	193683 (0.414)	193576 (0.377)	106.8	192848
Leuven2	112454.2 (0.954)	112145 (0.677)	121	112454.2 (0.767)	112027 (0.571)	141.4	111391
Antwerp1	479808.4 (0.53)	479551 (0.476)	98.4	479808.4 (0.514)	479546 (0.475)	119.8	477277
Antwerp2	294414.8 (1.052)	294173 (0.969)	104.4	294414.8 (1.052)	294100 (0.944)	131	291350
Ghent1	472596 (0.653)	472507 (0.634)	105.4	472596 (0.669)	472460 (0.624)	133.2	469531
Ghent2	261645.2 (1.512)	261346 (1.396)	115.2	261645.2 (1.412)	261134 (1.314)	149.4	257748
Brussels1	506761.8 (1.005)	506609 (0.975)	102.6	506761.8 (1.001)	506597 (0.972)	142.4	501719
Brussels2	351955.2 (1.878)	351461 (1.735)	113.4	351955.2 (1.882)	351590 (1.772)	151	345468
Flanders1	7294292 (0.748)	7291040 (0.703)	134.4	7294292 (0.708)	7289290 (0.679)	184.6	7240118
Flanders2	4464854 (2.095)	4462590 (2.043)	144.4	4464854 (2.073)	4461230 (2.012)	206.2	4373244
Average Gap	1.086		112.96	1.049		146.58	
Median Gap	0.980			0.884			

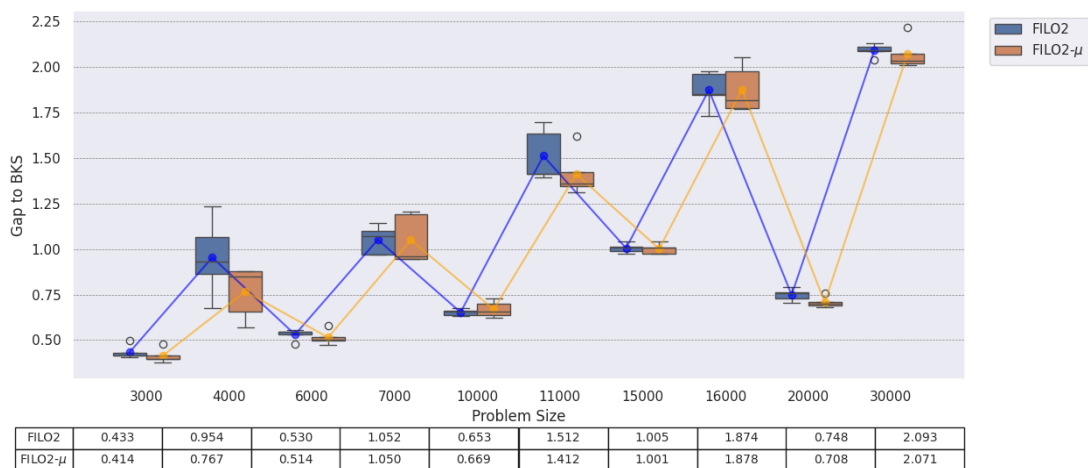


Figure 7: Comparison performance of FILO2 on \mathbb{B} instances.

Moreover, Table 3 presents the average gap to the BKS on the \mathbb{X} instances, categorized by different customer distribution: Random (R), Clustered (C), and Random-Clustered (RC). The goal is to evaluate how variations in

customer spatial distribution affect the performance of the proposed hybrid learning-based mechanisms compared to the baseline FILO2 algorithm. In the Random (R) distribution, where customers are uniformly spread across the area, most hybrid variants (FILO2- α , FILO2- β) slightly better than the baseline. FILO2- μ matches the baseline performance, while other variants show minor degradations. In the Clustered (C) case, the performance slightly worsens for most variants. However, FILO2- μ achieves the lowest gap of 0.373%, outperforming the baseline. Lastly, in the Random-Clustered (RC) scenario, FILO2- α , and FILO2- β all achieve matches the baseline performance. Furthermore, Table 4 presents a detailed comparison between the baseline FILO2 algorithm and the proposed hybrid variant FILO2- μ on all very large-scale instances from the \mathbb{B} dataset.

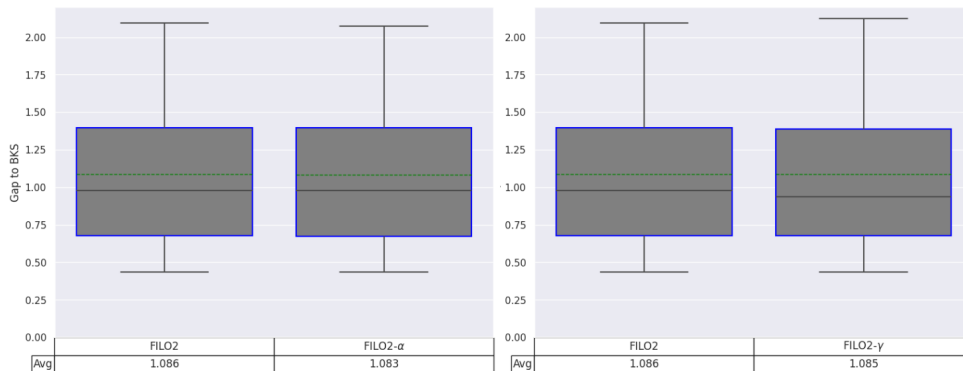


Figure 8: Boxplot of the performance of the hybrid FILO2 variants α and γ on \mathbb{B} instances.

Overall, FILO2- μ consistently outperforms the baseline in terms of both average and best gap. These performance gains come with a slight increase in computational time, primarily due to the inference overhead introduced by the deep learning-based selector f_θ used in variant μ . Then, in Figure 8 for baseline FILO2, on \mathbb{B} instances, the one-tailed Wilcoxon signed-rank test accept Hypothesis H_0 with p -value = 0.08986 (> 0.05) for variant α and p -value = 0.5 (> 0.05) for variant γ , indicating that proposed hybrid variant α and γ did not significantly improve the performance of the baseline FILO2 when solving \mathbb{B} instances. Moreover, in Figure 9 for baseline FILO2, on \mathbb{B} instances, the one-tailed Wilcoxon signed-rank test rejects Hypothesis H_0 with p -value = 0.0186 (< 0.05), indicating that proposed hybrid variant μ significantly improve the baseline FILO2 when solving \mathbb{B} instances.

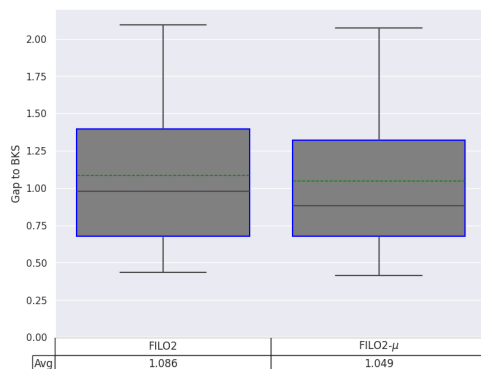


Figure 9: Boxplot of the performance of the hybrid FILO2 variants μ on \mathbb{B} instances.

5.2 Generalization Baseline HGS

To assess the generalization capability of the proposed hybrid mechanism, we applied the μ variant in HGS to solve the \mathbb{X} instances. This is because, as shown in Section 5.1, the μ variant is the only one that achieves a statistically significant improvement over FILO2, particularly when solving very large instances. Therefore, we explored the generalizability of the μ variant using a different baseline algorithm. As described in Section 2, FILO2 and HGS

Algorithm 2 The Edge-Selector f_θ variant μ applied in HGS.

Input: Problem instance: P

Output: Solution: S

```

1: procedure HYBRID-HGS( $P$ )
2:    $\mathbf{P} \leftarrow \text{INITIALPOPULATION}(P)$  ▷ random solutions improved by local search
3:   while  $t < T_{max}$  do
4:      $S_0 \leftarrow \text{GETBESTSOL}(\mathbf{P})$  ▷ best feasible solution as the refereed solution
5:      $\mathbf{P} \leftarrow \mathbf{P} \cup f_\theta(S_0)$  ▷ edge-labeled refereed solution in  $\mathbf{P}$ 
6:      $(P_1, P_2) \leftarrow \text{SELECTPARENTSOLUTIONS}(\mathbf{P})$ 
7:      $C \leftarrow \text{CROSSOVER}(P_1, P_2)$ ;
8:      $C' \leftarrow \text{LOCALSEARCHIMPROVEMENT}(C)$ 
9:      $\mathbf{P} \leftarrow \mathbf{P} \cup C'$ 
10:    if  $\neg \text{FEASIBLE}(C')$  then
11:      if  $\mathcal{R} < 0.5$  then ▷ random probability 50%
12:         $C'' \leftarrow \text{LOCALSEARCH}(C')$ 
13:         $\mathbf{P} \leftarrow \mathbf{P} \cup C''$ 
14:      end if
15:    end if
16:    if  $\text{SIZE}(\mathbf{P}) > \mu$  then ▷ maximum subpopulation size reached
17:       $\text{PRUNESURVIVORSBASEDONFITNESS}(\mathbf{P})$ 
18:       $\text{PENALTYADJUSTMENT}(\mathbf{P})$ 
19:    end if
20:     $\text{PENALTYADJUSTMENT}(\mathbf{P})$ 
21:  end while
22: end procedure

```

are structurally very different. HGS (Vidal, 2022) evolves a diverse population of solutions that comprises both feasible and infeasible individuals, such that $\mathbf{P} = \mathbf{P}_{\text{feas}} \cup \mathbf{P}_{\text{infeas}}$, and improves solution quality via recombination and local search operations.

In contrast, FILO2 refines a single incumbent solution through successive local search steps, using a simulated annealing acceptance criterion to maintain search diversity (Accorsi and Vigo, 2021). These structural differences provide a basis for testing the generalization ability of the proposed mechanism across different metaheuristic baselines. The pseudocode for the proposed hybrid edge selector mechanism integrated with the baseline HGS algorithm is presented in Algorithm 2. After an initial population is generated, the algorithm iteratively produces new solutions by selecting two parents, P_1 and P_2 , recombining them to create a new solution C , improving this solution via local search, and inserting the result back into the population.

This process is repeated until a termination criterion is met, which, in this research, is defined by a predefined time limit T_{max} (Vidal, 2022). In this framework, the selector marks the best feasible solution from the initial population as the reference solution S_0 . This solution is then input into the selector f_θ , where all edges in S_0 are labeled to guide the local search for improving all solutions in \mathbf{P} . Furthermore, whenever a specified number of consecutive iterations N_{IT} without improvement is reached, the algorithm regenerates the population. At this point, the selector f_θ also performs predictions again using a new reference solution from the newly generated population. Prior to conducting experiments on the \mathbb{X} instances, we set the threshold parameters as follows: $t = 0.75$ and $p_\Theta = 0.7$ for instances with $N < 500$, and $t = 0.85$ for larger instances. The experimental setup follows the configuration used in HGS (Vidal, 2022), with the maximum runtime defined as $T_{\text{max}} = N \times 2.4$ seconds for all \mathbb{X} instances.

Computational results Table 5 presents a comparative performance summary between the baseline HGS and the proposed hybrid variant HGS- μ that incorporates the graph learning as the baseline learning model (as

Table 5: Summary performances variant μ on HGS with $T_{max} = N \times 240/100$.

Problem Size	HGS		HGS- μ	
	Avg Gap	Best Gap	Avg Gap	Best Gap
101 - 200	0.005	0.002	0.005	0.001
204 - 491	0.071	0.039	0.061	0.032
502 - 1001	0.268	0.199	0.239	0.173
Average Gap	0.120		0.105	
Median Gap	0.059		0.046	

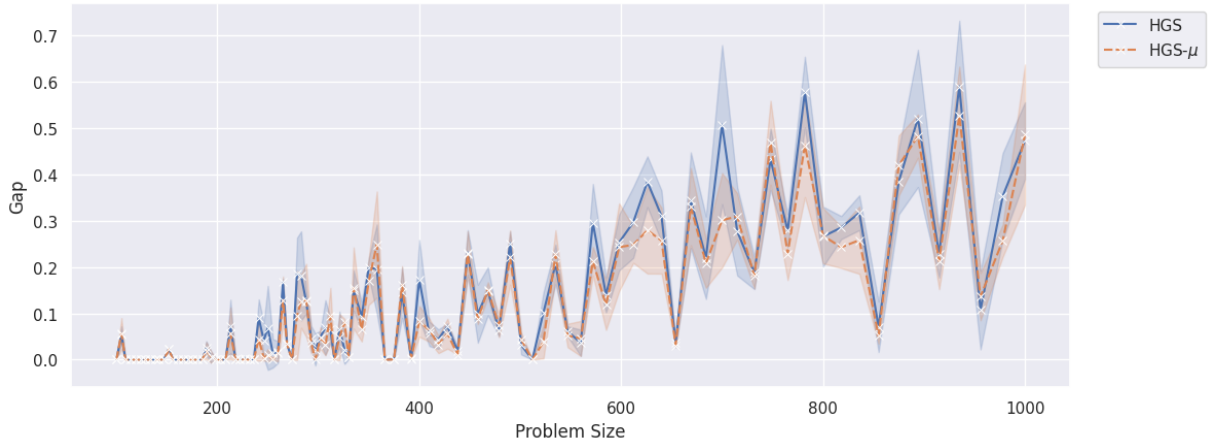


Figure 10: Comparison performance of HGS on \mathbb{X} instances.

summarized in Table 1, similar with baseline FILO2). The table reports results over three instance size categories from the \mathbb{X} benchmark set, where each configuration was evaluated under a similar maximum computational time $T_{max} = N \times \frac{240}{100}$.

Table 6: Performance on \mathbb{X} instances with varying customer distributions.

Customer Distribution	HGS	HGS- μ
Random (R)	0.105	0.092
Clustered (C)	0.110	0.098
Random-Clustered (RC)	0.128	0.113

Across all problem sizes, HGS- μ almost consistently improves the solution quality compared to the baseline HGS. For medium-sized instances (with 204 to 491 nodes), the average gap is reduced from 0.071% to 0.061%, and for large instances (with 502 to 1001 nodes), the improvement is more pronounced, with the average gap reduced from 0.268% to 0.239%. While both methods perform nearly similar on small instances, HGS- μ achieves a slightly better in best resulted solution. The overall average gap across all instance sizes is improved, indicating an enhancement in solution quality. Further, Table 6 presents a comparative evaluation of the baseline HGS and the proposed hybrid variant HGS- μ , across different customer distribution patterns on \mathbb{X} benchmark instances. Across all cases, HGS- μ improves the baseline HGS. Specifically, in Random instances, HGS- μ achieves a gap, improving upon the baseline. For Clustered distributions, HGS- μ also yields a better gap, compared the baseline. As shown in Figure 11, for the baseline HGS on the \mathbb{X} instances, the one-tailed Wilcoxon signed-rank test rejects Hypothesis H_0 with a p -value of 0.000056 (< 0.05), suggesting that the proposed hybrid variant μ statistically improves the performance of the baseline HGS on these instances. Furthermore, we compare the proposed method with other state-of-the-art metaheuristic solvers for the CVRP.

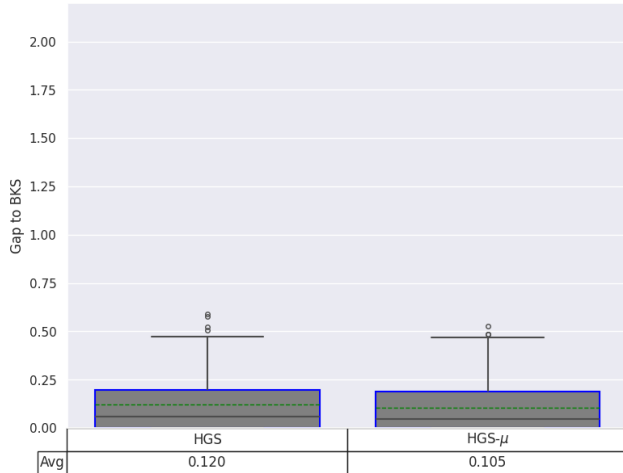


Figure 11: Boxplot of the performance of the hybrid HGS variants μ on \mathbb{X} instances.

As summarized in Table 7, we evaluate its performance against several well-known solvers: LKH⁶ (Helsgaun, 2017), SISRs⁷ (Christiaens and Vanden Berghe, 2020), HGS⁸ (Vidal, 2022), and the general commercial solver Hexaly⁹. All algorithms were evaluated under equivalent stopping criteria, with the maximum runtime set to $T_{\max} = N \times 240/100$ seconds.

Table 7: Comparison of solution quality with $T_{\max} = N \times 240/100$ on \mathbb{X} instances.

Measurement	LKH-3	SISRs	Hexaly	HGS	HGS- μ
Average Gap	1.029	0.194	1.731	0.120	0.105
Median Gap	0.898	0.170	1.120	0.059	0.049

From Table 7, it can be observed that although HGS already outperforms other metaheuristic solvers, the proposed hybrid mechanism achieves even better performance than HGS and indeed surpasses all other compared solvers. This demonstrates the capability of the proposed hybrid mechanism further to enhance the performance of a state-of-the-art baseline metaheuristic.

5.3 Generalization for VRP with Time Windows

To further evaluate the generalizability of the proposed hybrid mechanism, we conducted experiments on a more complex variant of the *Vehicle Routing Problems* (VRPs), namely the Capacitated VRP with Time Windows (CVRPTW) (Solomon, 1987). For this purpose, we integrated the proposed selector f_{θ} into the baseline HGS-TW (Kool et al., 2022b). Since the baseline HGS-TW already demonstrates strong performance on small- and medium-sized instances (Kool et al., 2022b), our focus is placed on testing the hybrid variant μ on a subset of the Gehring & Homberger benchmark instances (Gehring and Homberger, 1999). Specifically, we selected large-scale instances containing 800 and 1,000 customer nodes from the C, R, and RC sets, which are categorized based on customer distribution. In this setup, we applied variant μ within HGS-TW to solve the selected CVRPTW instances, using a decision threshold of $t = 0.85$ and an aspiration parameter of $p_{\Theta} = 0.6$. The integration mechanism mirrors the one used for the CVRP experiments: the best feasible solution from the initial population is selected as the reference solution S_0 , which is then passed to the selector f_{θ} . Additionally, if a predefined number of non-improving iterations N_{IT} is reached, the population is regenerated, and the selector f_{θ} re-evaluates a new reference solution from this updated population.

⁶LKH-3.0.9: <http://webhotel4.ruc.dk/~keld/research/LKH-3/>

⁷Results reported in Vidal, 2022

⁸HGS-CVRP: <https://github.com/vidalt/HGS-CVRP>

⁹Hexaly 13.0: <https://www.hexaly.com>

Table 8: Summary performances variant μ on HGS-TW with $T_{\max} = N \times 240/100$.

Problem Size	HGS-TW		HGS-TW- μ	
	Avg Gap	Best Gap	Avg Gap	Best Gap
800	0.509	0.353	0.437	0.304
1000	0.790	0.578	0.675	0.497
Average Gap	0.649		0.556	
Median Gap	0.628		0.547	

Computational results The experimental results summarized in Table 8 and Table 9 highlight the effectiveness of the hybrid μ variant when integrated into the baseline HGS-TW for solving Gehring & Homberger instances (Gehring and Homberger, 1999). As shown in Table 8, HGS-TW- μ consistently outperforms the baseline across large problem sizes. Additionally, Table 9 demonstrates the method’s robustness across different customer distributions. The hybrid approach yields improvements in all scenarios, with particularly notable reductions in the average gap for Random (R) and Random-Clustered (RC) distributions.

Table 9: Performance of HGS-TW with varying customer distributions.

Customer Distribution	HGS-TW	HGS-TW- μ
Random (R)	0.923	0.765
Clustered (C)	0.184	0.153
Random-Clustered (RC)	0.841	0.749

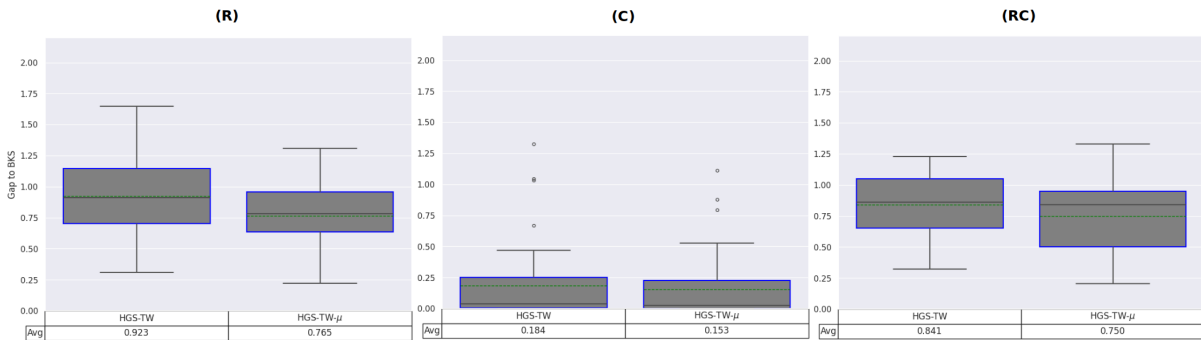


Figure 12: Comparison performance of HGS-TW.

As shown in Table 8, HGS-TW- μ outperforms the baseline across large problem sizes. Additionally, Table 9 demonstrates the improvement across different customer distributions. The hybrid approach yields improvements in all scenarios, with particularly notable reductions in the average gap for Random (R) and Random-Clustered (RC) distributions. As shown in Table 9, the one-tailed Wilcoxon signed-rank test rejects Hypothesis H_0 for the baseline HGS-TW on a subset of the Gehring & Homberger instances (Gehring and Homberger, 1999). Specifically, statistically significant improvements were observed with p -values of 0.000002 (< 0.05) for the random distribution, 0.00177 (< 0.05) for the clustered distribution, and 0.00006 (< 0.05) for the random-clustered distribution. These results demonstrate that the proposed hybrid variant μ significantly enhances the performance of the baseline across all types of customer distributions.

6 Conclusion

In this paper, we introduced a novel iterative learning-based hybrid optimization framework aimed at enhancing local search performance within metaheuristic solvers. At the core of the proposed approach is an edge selector model that classifies solution edges to identify and prohibit unpromising moves, thereby reducing the neighborhood search space and filtering out unnecessary local search operations. This model operates within an in-loop, machine learning-guided optimization framework that enables adaptive, data-driven guidance through repeated decision inference. We implemented the selector using two learning paradigms: tabular binary classifiers (GBT and FNN) and Graph Neural Network (GNN), with both deterministic and stochastic thresholding techniques applied to address class imbalance. To evaluate scalability, we applied the framework to CVRP instances with customer sizes ranging from 100 to 30,000. The results show statistically significant improvements for both medium and large scale problem instances. To assess generalizability, we integrated the mechanism into two structurally distinct metaheuristics, HGS as a population-based method and FILO2 as a single-solution-based method. Both showed consistent and statistically significant performance gains when augmented with the hybrid mechanism. Finally, we extended the approach to solve CVRPTW using HGS-TW as the baseline. The results demonstrated that the hybrid mechanism significantly improves the solver’s performance across all customer distribution types on large instances, confirming the robustness of the proposed approach.

A Appendix

A.1 Edge-Solution Features for Tabular Learning

Let R denote the set of all routes in a given solution. Each route, denoted as $r_k = \{c_1, c_2, \dots, c_k\} \in R$, represents an ordered sequence of customer nodes that must be visited consecutively. The relationship between any two nodes c_i and c_j in terms of their proximity within the problem space is captured by the neighborhood rank \mathcal{R}_{ij} , which reflects the relative closeness of node c_j to node c_i based on distance or similarity metrics. Each route $r_k \in R$ consists of a series of directed edges forming the path $(D, c_1), (c_1, c_2), \dots, (c_k, D) \in E$, where D denotes the depot serving as both the starting and ending point of the route. The Euclidean distance between any two customer nodes c_j and c_k is denoted by $d(c_j, c_k)$, computed using their spatial coordinates. Specifically, the horizontal and vertical positions of node c_k are denoted by $x(c_k)$ and $y(c_k)$, respectively. In addition, each customer node c_j is associated with a demand value, represented as $q(c_j)$, which indicates the quantity of goods required by that customer. If nodes c_i and c_j are connected by an edge in a route $r_k \in R$ within a solution S , then this edge can be characterized by a set of solution-specific features, including:

- percentage load, x_1

$$x_1 := \frac{(q(c_i) + q(c_j))}{\sum_N q(c)} \quad (11)$$

- utilization edge, x_2

$$x_2 := \frac{(q(c_i) + q(c_j))}{\sum_{R_k} q(c)} \quad (12)$$

- rank of the neighborhood, x_3

$$x_3 := \mathcal{R}_{ij} \cdot \delta_{\mathcal{R}_{ij} \leq \Gamma} + (-1) \cdot (1 - \delta_{\mathcal{R}_{ij} \leq \Gamma}) \quad (13)$$

- percentage distance, x_4

$$x_4 := \frac{d(c_i, c_j)}{S} \quad (14)$$

The term $\delta_{\mathcal{R}_{ij} \leq \Gamma}$ is used for extending the Kronecker delta notation to include a special condition, δ_{cond} , which equal to 1 if the condition is met and 0 otherwise. For x_3 , rank of the neighborhood, we adjust the granularity Γ of the baseline algorithm. To ensure this, the value of x_3 will be set to -1 whenever $\mathcal{R}_{ij} > 25$. This transformation respects the granularity mechanism of the local search used in the baseline algorithm while maintain the consistency in feature representation.

A.2 Detailed Experiment using Baseline HGS

Table 10: Detailed performances variant μ with HGS on \mathbb{X} instances.

Instance	HGS		HGS- μ		BKS
	Avg Gap	Best Gap	Avg Gap	Best Gap	
X-n101-k25	27591 (0.0000)	27591 (0.0000)	27591 (0.0000)	27591 (0.0000)	27591
X-n106-k14	26376.2 (0.0539)	26370 (0.0303)	26376.8 (0.0561)	26362 (0.0000)	26362
X-n110-k13	14971 (0.0000)	14971 (0.0000)	14971 (0.0000)	14971 (0.0000)	14971
X-n115-k10	12747 (0.0000)	12747 (0.0000)	12747 (0.0000)	12747 (0.0000)	12747
X-n120-k6	13332 (0.0000)	13332 (0.0000)	13332 (0.0000)	13332 (0.0000)	13332
X-n125-k30	55539 (0.0000)	55539 (0.0000)	55539 (0.0000)	55539 (0.0000)	55539
X-n129-k18	28940 (0.0000)	28940 (0.0000)	28940 (0.0000)	28940 (0.0000)	28940
X-n134-k13	10916 (0.0000)	10916 (0.0000)	10916 (0.0000)	10916 (0.0000)	10916
X-n139-k10	13590 (0.0000)	13590 (0.0000)	13590 (0.0000)	13590 (0.0000)	13590
X-n143-k7	15700 (0.0000)	15700 (0.0000)	15700 (0.0000)	15700 (0.0000)	15700
X-n148-k46	43448 (0.0000)	43448 (0.0000)	43448 (0.0000)	43448 (0.0000)	43448
X-n153-k22	21225 (0.0236)	21225 (0.0236)	21224.8 (0.0226)	21224 (0.0189)	21220
X-n157-k13	16876 (0.0000)	16876 (0.0000)	16876 (0.0000)	16876 (0.0000)	16876
X-n162-k11	14138 (0.0000)	14138 (0.0000)	14138 (0.0000)	14138 (0.0000)	14138
X-n167-k10	20557 (0.0000)	20557 (0.0000)	20557 (0.0000)	20557 (0.0000)	20557
X-n172-k51	45607 (0.0000)	45607 (0.0000)	45607 (0.0000)	45607 (0.0000)	45607
X-n176-k26	47812 (0.0000)	47812 (0.0000)	47812 (0.0000)	47812 (0.0000)	47812
X-n181-k23	25569 (0.0000)	25569 (0.0000)	25569 (0.0000)	25569 (0.0000)	25569
X-n186-k15	24145 (0.0000)	24145 (0.0000)	24145 (0.0000)	24145 (0.0000)	24145
X-n190-k8	16984.2 (0.0247)	16980 (0.0000)	16983.4 (0.0200)	16980 (0.0000)	16980
X-n195-k51	44227.4 (0.0054)	44225 (0.0000)	44227.4 (0.0054)	44225 (0.0000)	44225
X-n200-k36	58578 (0.0000)	58578 (0.0000)	58578 (0.0000)	58578 (0.0000)	58578
X-n204-k19	19565 (0.0000)	19565 (0.0000)	19565 (0.0000)	19565 (0.0000)	19565
X-n209-k16	30656 (0.0000)	30656 (0.0000)	30656 (0.0000)	30656 (0.0000)	30656
X-n214-k11	10863.8 (0.0718)	10856 (0.0000)	10862.2 (0.0571)	10859 (0.0276)	10856
X-n219-k73	117595 (0.0000)	117595 (0.0000)	117597.2 (0.0019)	117595 (0.0000)	117595
X-n223-k34	40437 (0.0000)	40437 (0.0000)	40437 (0.0000)	40437 (0.0000)	40437
X-n228-k23	25743 (0.0039)	25743 (0.0039)	25742.2 (0.0008)	25742 (0.0000)	25742
X-n233-k16	19230 (0.0000)	19230 (0.0000)	19230 (0.0000)	19230 (0.0000)	19230
X-n237-k14	27042 (0.0000)	27042 (0.0000)	27042 (0.0000)	27042 (0.0000)	27042
X-n242-k48	82825.6 (0.0901)	82768 (0.0205)	82787.6 (0.0442)	82768 (0.0205)	82751
X-n247-k50	37289.6 (0.0419)	37278 (0.0107)	37275.4 (0.0038)	37274 (0.0000)	37274
X-n251-k28	38710.6 (0.0688)	38684 (0.0000)	38687.8 (0.0098)	38684 (0.0000)	38684
X-n256-k16	18841.6 (0.0138)	18839 (0.0000)	18839 (0.0000)	18839 (0.0000)	18839
X-n261-k13	26562.4 (0.0166)	26558 (0.0000)	26561.6 (0.0136)	26558 (0.0000)	26558
X-n266-k58	75604.2 (0.1672)	75595 (0.1550)	75575 (0.1285)	75517 (0.0517)	75478
X-n270-k35	35303 (0.0340)	35303 (0.0340)	35303 (0.0340)	35303 (0.0340)	35291
X-n275-k28	21245 (0.0000)	21245 (0.0000)	21245 (0.0000)	21245 (0.0000)	21245
X-n280-k17	33565.2 (0.1857)	33536 (0.0985)	33535 (0.0955)	33506 (0.0090)	33503
X-n284-k15	20251.6 (0.1811)	20217 (0.0099)	20240.6 (0.1266)	20228 (0.0643)	20215
X-n289-k60	95270.8 (0.1259)	95238 (0.0914)	95273 (0.1282)	95183 (0.0336)	95151
X-n294-k50	47182.2 (0.0450)	47167 (0.0127)	47178.4 (0.0369)	47161 (0.0000)	47161
X-n298-k31	34238.6 (0.0222)	34231 (0.0000)	34231 (0.0000)	34231 (0.0000)	34231
X-n303-k21	21746.6 (0.0488)	21743 (0.0322)	21746.2 (0.0469)	21739 (0.0138)	21736

Table 11: Detailed performances variant μ with HGS on \mathbb{X} instances (continue).

Instance	HGS		HGS- μ		BKS
	Avg Gap	Best Gap	Avg Gap	Best Gap	
X-n308-k13	25877 (0.0696)	25862 (0.0116)	25867.2 (0.0317)	25862 (0.0116)	25859
X-n313-k71	94104.2 (0.0651)	94085 (0.0447)	94132.2 (0.0949)	94044 (0.0011)	94043
X-n317-k53	78355 (0.0000)	78355 (0.0000)	78355 (0.0000)	78355 (0.0000)	78355
X-n322-k28	29853.6 (0.0657)	29834 (0.0000)	29848.6 (0.0489)	29834 (0.0000)	29834
X-n327-k20	27538 (0.0218)	27532 (0.0000)	27554.4 (0.0814)	27553 (0.0763)	27532
X-n331-k15	31103.4 (0.0045)	31103 (0.0032)	31103.4 (0.0045)	31103 (0.0032)	31102
X-n336-k84	139318.8 (0.1494)	139249 (0.0992)	139326.4 (0.1548)	139192 (0.0582)	139111
X-n344-k43	42089.2 (0.0932)	42072 (0.0523)	42077.4 (0.0652)	42061 (0.0262)	42050
X-n351-k40	25947.6 (0.1993)	25939 (0.1660)	25940 (0.1699)	25922 (0.1004)	25896
X-n359-k29	51605.8 (0.1957)	51571 (0.1281)	51633.2 (0.2489)	51578 (0.1417)	51505
X-n367-k17	22814 (0.0000)	22814 (0.0000)	22814 (0.0000)	22814 (0.0000)	22814
X-n376-k94	147716 (0.0020)	147713 (0.0000)	147714 (0.0007)	147713 (0.0000)	147713
X-n384-k52	66035.8 (0.1453)	65975 (0.0531)	66046.6 (0.1617)	66003 (0.0955)	65940
X-n393-k38	38260 (0.0000)	38260 (0.0000)	38261.2 (0.0031)	38260 (0.0000)	38260
X-n401-k29	66277.4 (0.1729)	66213 (0.0756)	66217.8 (0.0828)	66180 (0.0257)	66163
X-n411-k19	19723 (0.0558)	19719 (0.0355)	19724.6 (0.0639)	19718 (0.0304)	19712
X-n420-k130	107845.8 (0.0443)	107818 (0.0186)	107833.6 (0.0330)	107824 (0.0241)	107798
X-n429-k61	65496.4 (0.0724)	65490 (0.0626)	65485.8 (0.0562)	65464 (0.0229)	65449
X-n439-k37	36397.8 (0.0187)	36395 (0.0110)	36395 (0.0110)	36395 (0.0110)	36391
X-n449-k29	55361 (0.2317)	55343 (0.1992)	55359.2 (0.2285)	55334 (0.1829)	55233
X-n459-k26	24163 (0.0994)	24139 (0.0000)	24160 (0.0870)	24157 (0.0746)	24139
X-n469-k138	222152.2 (0.1480)	222062 (0.1073)	222158.6 (0.1508)	222093 (0.1213)	221824
X-n480-k70	89506.8 (0.0646)	89499 (0.0559)	89515 (0.0738)	89491 (0.0470)	89449
X-n491-k59	66654.4 (0.2518)	66626 (0.2091)	66633.8 (0.2208)	66590 (0.1549)	66487
X-n502-k39	69248.2 (0.0321)	69234 (0.0116)	69256.4 (0.0439)	69238 (0.0173)	69226
X-n513-k21	24201 (0.0000)	24201 (0.0000)	24201 (0.0000)	24201 (0.0000)	24201
X-n524-k153	154750.2 (0.1017)	154648 (0.0356)	154652.2 (0.0383)	154610 (0.0110)	154593
X-n536-k96	95063.4 (0.2060)	95042 (0.1834)	95084 (0.2277)	95001 (0.1402)	94868
X-n548-k50	86753.2 (0.0614)	86745 (0.0519)	86745.4 (0.0524)	86709 (0.0104)	86700
X-n561-k42	42732.6 (0.0365)	42719 (0.0047)	42736.6 (0.0459)	42719 (0.0047)	42717
X-n573-k30	50823 (0.2960)	50777 (0.2052)	50780.8 (0.2127)	50762 (0.1756)	50673
X-n586-k159	190582.8 (0.1402)	190475 (0.0835)	190541.2 (0.1183)	190449 (0.0699)	190316
X-n599-k92	108725.8 (0.2534)	108663 (0.1955)	108714.6 (0.2431)	108581 (0.1199)	108451
X-n613-k62	59711.6 (0.2966)	59646 (0.1864)	59682.8 (0.2483)	59658 (0.2066)	59535
X-n627-k43	62403 (0.3845)	62354 (0.3056)	62337.8 (0.2796)	62284 (0.1930)	62164
X-n641-k35	63891.6 (0.3102)	63869 (0.2748)	63858 (0.2575)	63815 (0.1900)	63694
X-n655-k131	106818.8 (0.0363)	106810 (0.0281)	106813 (0.0309)	106809 (0.0272)	106780
X-n670-k130	146836 (0.3444)	146675 (0.2344)	146815.8 (0.3306)	146701 (0.2522)	146332
X-n685-k75	68355.4 (0.2205)	68284 (0.1158)	68347 (0.2082)	68292 (0.1276)	68205
X-n701-k44	82339 (0.5078)	82201 (0.3393)	82169.8 (0.3013)	82107 (0.2246)	81923
X-n716-k35	43507.4 (0.2775)	43446 (0.1360)	43521.4 (0.3098)	43494 (0.2466)	43387
X-n733-k159	136445.6 (0.1877)	136397 (0.1520)	136436.4 (0.1809)	136387 (0.1447)	136190
X-n749-k98	77648.8 (0.4330)	77600 (0.3699)	77676.4 (0.4687)	77597 (0.3660)	77314
X-n766-k71	114773 (0.2787)	114739 (0.2490)	114715.8 (0.2287)	114648 (0.1695)	114454
X-n783-k48	72812.6 (0.5782)	72763 (0.5097)	72729.4 (0.4633)	72637 (0.3357)	72394
X-n801-k40	73500 (0.2660)	73431 (0.1719)	73501.4 (0.2679)	73462 (0.2142)	73305
X-n819-k171	158572.4 (0.2855)	158511 (0.2466)	158505.2 (0.2430)	158439 (0.2011)	158121
X-n837-k142	194352.4 (0.3176)	194261 (0.2705)	194237.4 (0.2583)	194035 (0.1538)	193737
X-n856-k95	89028.2 (0.0710)	88990 (0.0281)	89011.2 (0.0519)	88993 (0.0315)	88965
X-n876-k59	99681 (0.3847)	99576 (0.2790)	99715.6 (0.4195)	99602 (0.3051)	99299
X-n895-k37	54140.8 (0.5214)	54063 (0.3769)	54120.2 (0.4831)	54101 (0.4475)	53860
X-n916-k207	329930.2 (0.2282)	329667 (0.1482)	329879.8 (0.2129)	329658 (0.1455)	329179
X-n936-k151	133508.8 (0.5905)	133314 (0.4438)	133424.8 (0.5273)	133176 (0.3398)	132725
X-n957-k87	85556.8 (0.1074)	85514 (0.0573)	85581.6 (0.1364)	85540 (0.0878)	85465
X-n979-k58	119407 (0.3530)	119326 (0.2849)	119292.8 (0.2570)	119257 (0.2269)	118987
X-n1001-k43	72701.4 (0.4732)	72631 (0.3759)	72710.8 (0.4862)	72620 (0.3607)	72359
Average Gap	0.120		0.105		
Median Gap	0.059		0.046		

A.3 Detailed Experiment using Baseline HGS-TW

A.3.1 Experiment on Clustered (C) Group: Set 1 and Set 2

Table 12: Performances variant μ on HGS-TW on clustered instances set 1 and set 2.

Instance	HGS-TW		HGS-TW- μ		BKS	Instance	HGS-TW		HGS-TW- μ		BKS
	Avg Gap	Best Gap	Avg Gap	Best Gap			Avg Gap	Best Gap	Avg Gap	Best Gap	
C1_8_1	11632.68 (0.007)	11631.9 (0.000)	11633.04 (0.010)	11631.9 (0.000)	11631.9	C2_8_1	11632.68 (0.007)	11631.9 (0.000)	11633.04 (0.010)	11631.9 (0.000)	11631.9
C1_8_1	25156.9 (0.000)	25156.9 (0.000)	25156.90 (0.000)	25156.9 (0.000)	25156.9	C2_8_1	11632.68 (0.007)	11631.9 (0.000)	11633.04 (0.010)	11631.9 (0.000)	11631.9
C1_8_2	24995.76 (0.087)	24978.9 (0.019)	24999.42 (0.101)	24983.7 (0.038)	24974.1	C2_8_2	11395.24 (0.006)	11394.6 (0.001)	11394.86 (0.003)	11394.5 (0.000)	11394.5
C1_8_3	24226.98 (0.293)	24205.4 (0.204)	24219.80 (0.264)	24185.3 (0.121)	24156.1	C2_8_3	11138.16 (0.001)	11138.1 (0.000)	11138.24 (0.001)	11138.2 (0.001)	11138.1
C1_8_4	23855.1 (0.243)	23831.2 (0.142)	23861.74 (0.271)	23850.3 (0.223)	23797.3	C2_8_4	10662.26 (0.213)	10653.6 (0.132)	10659.46 (0.187)	10647.9 (0.078)	10639.6
C1_8_5	25138.6 (0.000)	25138.6 (0.000)	25138.60 (0.000)	25138.6 (0.000)	25138.6	C2_8_5	11395.76 (0.001)	11395.6 (0.000)	11395.60 (0.000)	11395.6 (0.000)	11395.6
C1_8_6	25133.3 (0.000)	25133.3 (0.000)	25133.30 (0.000)	25133.3 (0.000)	25133.3	C2_8_6	11318.84 (0.022)	11318.2 (0.017)	11319.54 (0.029)	11318.2 (0.017)	11316.3
C1_8_7	25127.3 (0.000)	25127.3 (0.000)	25127.30 (0.000)	25127.3 (0.000)	25127.3	C2_8_7	11334.88 (0.017)	11332.9 (0.000)	11334.36 (0.013)	11332.9 (0.000)	11332.9
C1_8_8	24892.3 (0.333)	24867.7 (0.234)	24880.54 (0.286)	24861.0 (0.207)	24809.7	C2_8_8	11136.78 (0.026)	11133.9 (0.000)	11139.28 (0.048)	11135.0 (0.010)	11133.9
C1_8_9	24275.18 (0.309)	24253 (0.217)	24282.06 (0.337)	24267.2 (0.276)	24200.4	C2_8_9	11141.84 (0.013)	11140.4 (0.000)	11141.50 (0.010)	11140.4 (0.000)	11140.4
C1_8_10	24114.12 (0.364)	24083.1 (0.235)	24081.06 (0.226)	24059.7 (0.137)	24026.7	C2_8_10	10947.98 (0.018)	10946.6 (0.005)	10948.78 (0.025)	10948.4 (0.022)	10946
C1_10_1	42444.8 (0.000)	42444.8 (0.000)	42444.80 (0.000)	42444.8 (0.000)	42444.8	C2_10_1	16841.1 (0.000)	16841.1 (0.000)	16841.10 (0.000)	16841.1 (0.000)	16841.1
C1_10_2	41450.68 (0.273)	41390 (0.126)	41434.02 (0.233)	41393.2 (0.134)	41337.8	C2_10_2	16469.26 (0.040)	16466.5 (0.024)	16468.30 (0.035)	16466.5 (0.024)	16462.6
C1_10_3	40327.56 (0.668)	40159.2 (0.248)	40271.06 (0.527)	40219.2 (0.397)	40060	C2_10_3	16042.26 (0.036)	16038 (0.009)	16039.16 (0.017)	16037.5 (0.006)	16036.5
C1_10_4	39618.56 (0.468)	39535.8 (0.258)	39582.70 (0.377)	39539.0 (0.266)	39434.1	C2_10_4	15484.64 (0.163)	15463.2 (0.024)	15477.56 (0.117)	15462.4 (0.019)	15459.5
C1_10_5	42434.8 (0.000)	42434.8 (0.000)	42434.80 (0.000)	42434.8 (0.000)	42434.8	C2_10_5	16536.88 (0.094)	16535.2 (0.084)	16524.88 (0.022)	16523.4 (0.013)	16521.3
C1_10_6	42437 (0.000)	42437 (0.000)	42437.00 (0.000)	42437.0 (0.000)	42437	C2_10_6	16300.58 (0.061)	16294 (0.020)	16298.60 (0.048)	16295.9 (0.032)	16290.7
C1_10_7	42421.5 (0.003)	42420.7 (0.001)	42420.72 (0.001)	42420.4 (0.000)	42420.4	C2_10_7	16381.48 (0.019)	16380.1 (0.010)	16379.84 (0.009)	16379.2 (0.005)	16378.4
C1_10_8	42082.86 (1.044)	42026.5 (0.909)	42013.94 (0.879)	41881.4 (0.560)	41648	C2_10_8	16037.54 (0.053)	16030.5 (0.009)	16031.98 (0.018)	16029.8 (0.004)	16029.1
C1_10_9	40822.48 (1.326)	40621.7 (0.827)	40735.96 (1.111)	40575.3 (0.712)	40288.4	C2_10_9	16084.4 (0.056)	16081.6 (0.039)	16087.72 (0.077)	16080.1 (0.029)	16075.4
C1_10_10	40228.02 (1.033)	40001.2 (0.463)	40133.58 (0.796)	40003.1 (0.468)	39816.8	C2_10_10	15741.88 (0.084)	15728.6 (0.000)	15737.96 (0.060)	15732.3 (0.024)	15728.6
Average Gap	0.322		0.270			0.047		0.036			
Median Gap	0.258		0.230			0.024		0.020			

A.3.2 Experiment on Random (R) Group: Set 1 and Set 2

Table 13: Performances variant μ on HGS-TW on random distribution instances set 1 and set 2.

Instance	HGS-TW		HGS-TW- μ		BKS	Instance	HGS-TW		HGS-TW- μ		BKS
	Avg Gap	Best Gap	Avg Gap	Best Gap			Avg Gap	Best Gap	Avg Gap	Best Gap	
R1_s_1	36537.54 (0.530)	36458.8 (0.313)	36541.32 (0.540)	36477.4 (0.364)	36345	R2_s_1	25061.74 (0.392)	25022 (0.233)	11676.26 (0.381)	11664.7 (0.282)	24963.8
R1_s_2	32731.3 (1.406)	32634.6 (1.106)	32615.62 (1.047)	32522.9 (0.760)	32277.6	R2_s_2	21395.4 (0.390)	21341.6 (0.138)	11426.99 (0.285)	11411.1 (0.146)	21312.2
R1_s_3	29667.04 (1.249)	29641.6 (1.162)	29593.06 (0.996)	29567.2 (0.908)	29301.2	R2_s_3	17282.72 (0.309)	17259.9 (0.176)	11162.72 (0.221)	11151.0 (0.116)	17229.5
R1_s_4	27978.94 (0.881)	27900.6 (0.598)	27941.20 (0.745)	27910.2 (0.633)	27734.7	R2_s_4	13269.88 (0.890)	13218.8 (0.502)	10714.30 (0.702)	10681.2 (0.391)	13152.8
R1_s_5	33729.92 (0.704)	33658.2 (0.490)	33716.98 (0.666)	33650.8 (0.468)	33494	R2_s_5	22870.82 (0.330)	22854.6 (0.259)	11436.54 (0.359)	11416.7 (0.185)	22795.6
R1_s_6	31141.02 (0.870)	31076.8 (0.662)	31185.88 (1.015)	31081.0 (0.676)	30872.4	R2_s_6	19838.28 (0.495)	19786.7 (0.234)	11363.46 (0.417)	11334.1 (0.158)	19740.5
R1_s_7	29075.22 (0.994)	28979 (0.660)	29023.52 (0.815)	28972.4 (0.637)	28789	R2_s_7	16437.22 (0.526)	16411.2 (0.367)	11396.33 (0.560)	11381.8 (0.431)	16351.2
R1_s_8	27802.58 (0.700)	27731.8 (0.443)	27786.16 (0.640)	27760.0 (0.545)	27609.4	R2_s_8	12737.82 (1.001)	12713.7 (0.810)	11214.93 (0.728)	11174.2 (0.362)	12611.6
R1_s_9	32485.7 (0.708)	32445.2 (0.583)	32513.78 (0.795)	32456.1 (0.616)	32257.3	R2_s_9	21389.78 (0.503)	21376.4 (0.440)	11183.99 (0.391)	11157.4 (0.153)	21282.7
R1_s_10	31232.42 (1.016)	31165.5 (0.800)	31231.76 (1.014)	31168.0 (0.808)	30918.3	R2_s_10	20125.78 (0.809)	20101.7 (0.689)	11016.28 (0.642)	11002.6 (0.517)	19964.2
R1_10_1	53523.46 (0.938)	53443 (0.786)	53473.72 (0.844)	53409.9 (0.724)	53026.1	R2_10_1	37164.3 (0.768)	37088.4 (0.562)	16944.40 (0.613)	16911.0 (0.415)	36881
R1_10_2	49001.84 (1.534)	48863.2 (1.247)	48894.04 (1.310)	48766.5 (1.046)	48261.6	R2_10_2	31506.34 (0.846)	31452.4 (0.674)	16574.54 (0.680)	16549.6 (0.528)	31241.9
R1_10_3	45305.54 (1.415)	45111.9 (0.982)	45177.24 (1.128)	45049.3 (0.842)	44673.3	R2_10_3	24532.2 (0.546)	24447.3 (0.198)	16115.90 (0.495)	16077.2 (0.254)	24399
R1_10_4	42902.98 (1.089)	42839.7 (0.940)	42811.76 (0.874)	42759.7 (0.752)	42440.7	R2_10_4	18096.72 (1.602)	18015 (1.143)	15612.56 (0.990)	15536.9 (0.501)	17811.4
R1_10_5	50882.16 (0.943)	50698.1 (0.578)	50798.06 (0.776)	50714.2 (0.610)	50406.7	R2_10_5	34414.98 (0.827)	34374 (0.707)	16656.54 (0.819)	16634.7 (0.686)	34132.8
R1_10_6	47700.96 (1.647)	47471.1 (1.157)	47417.80 (1.043)	47268.2 (0.725)	46928.2	R2_10_6	29408.2 (0.973)	29270.5 (0.501)	16425.70 (0.829)	16413.8 (0.755)	29124.7
R1_10_7	44616.16 (1.406)	44516.6 (1.180)	44488.92 (1.117)	44257.9 (0.592)	43997.4	R2_10_7	23298.1 (0.848)	23222.3 (0.520)	16533.16 (0.945)	16444.8 (0.406)	23102.2
R1_10_8	42683.66 (0.956)	42657.2 (0.894)	42672.96 (0.931)	42556.1 (0.655)	42279.3	R2_10_8	17601.84 (1.138)	17557.7 (0.885)	16155.48 (0.788)	16109.8 (0.503)	17403.7
R1_10_9	49736.6 (1.167)	49589.3 (0.868)	49530.86 (0.749)	49390.7 (0.464)	49162.8	R2_10_9	32288.76 (0.932)	32224.3 (0.731)	16200.53 (0.778)	16180.7 (0.655)	31990.6
R1_10_10	48043.28 (1.433)	47954.5 (1.245)	47850.38 (1.026)	47761.0 (0.837)	47364.6	R2_10_10	30195.06 (1.188)	30063.2 (0.746)	15868.03 (0.886)	15801.7 (0.464)	29840.5
Average Gap	1.079		0.904			0.766		0.626			
Median Gap	1.005		0.903			0.818		0.661			

A.3.3 Experiment on Random-Clustered (RC) Group: Set 1 and Set 2

Table 14: Performances variant μ on HGS-TW on random-clustered instances set 1 and set 2.

Instance	HGS-TW		HGS-TW- μ		BKS	Instance	HGS-TW		HGS-TW- μ		BKS
	Avg Gap	Best Gap	Avg Gap	Best Gap			Avg Gap	Best Gap	Avg Gap	Best Gap	
RC1_s.1	30145.6 (0.644)	30081.8 (0.431)	30110.62 (0.527)	30048.8 (0.321)	29952.8	RC2_s.1	19283.8 (0.430)	19236.6 (0.184)	30044.93 (0.308)	30012.4 (0.199)	19201.3
RC1_s.2	28571.34 (0.994)	28557.4 (0.945)	28506.68 (0.766)	28453.0 (0.576)	28290.1	RC2_s.2	16763.38 (0.322)	16738.2 (0.172)	28347.80 (0.204)	28316.9 (0.095)	16709.5
RC1_s.3	27646.44 (0.724)	27521 (0.267)	27561.14 (0.413)	27497.3 (0.181)	27447.7	RC2_s.3	14080.86 (0.480)	14058.9 (0.323)	27556.29 (0.396)	27493.9 (0.168)	14013.6
RC1_s.4	26736.26 (0.674)	26667.5 (0.415)	26733.74 (0.665)	26684.8 (0.480)	26557.2	RC2_s.4	11049.64 (0.731)	11033.8 (0.587)	26727.88 (0.643)	26634.4 (0.291)	10969.4
RC1_s.5	29410.66 (0.653)	29364.4 (0.495)	29387.98 (0.575)	29352.3 (0.453)	29219.9	RC2_s.5	17550.06 (0.481)	17519.1 (0.303)	29319.74 (0.342)	29304.4 (0.289)	17466.1
RC1_s.6	29386.02 (0.814)	29339.4 (0.654)	29325.52 (0.607)	29266.1 (0.403)	29148.7	RC2_s.6	17276.54 (0.500)	17237.1 (0.270)	29266.61 (0.405)	29219.7 (0.244)	17190.6
RC1_s.7	28997.08 (0.916)	28974.6 (0.837)	28924.06 (0.661)	28891.2 (0.547)	28734	RC2_s.7	16500.96 (0.848)	16455.7 (0.571)	29010.38 (0.962)	28977.2 (0.846)	16362.2
RC1_s.8	28624.86 (0.827)	28546.8 (0.552)	28632.54 (0.854)	28610.2 (0.776)	28390	RC2_s.8	15673.4 (0.931)	15628 (0.639)	28646.94 (0.905)	28599.0 (0.736)	15528.8
RC1_s.9	28576.9 (0.866)	28435.8 (0.368)	28517.54 (0.656)	28383.5 (0.183)	28331.6	RC2_s.9	15267.8 (0.597)	15232.1 (0.362)	28409.82 (0.276)	28390.4 (0.208)	15177.2
RC1_s.10	28317.34 (0.528)	28214.2 (0.162)	28286.58 (0.419)	28269.7 (0.359)	28168.5	RC2_s.10	14502.68 (0.917)	14484.2 (0.788)	28407.40 (0.848)	28344.5 (0.625)	14370.9
RC1_10.1	46288.88 (1.088)	46175.5 (0.840)	46203.32 (0.901)	46124.2 (0.728)	45790.7	RC2_10.1	28407.04 (1.011)	28293.5 (0.608)	46202.91 (0.900)	46063.9 (0.597)	28122.6
RC1_10.2	44184.9 (1.160)	44135.7 (1.047)	44168.72 (1.123)	44076.4 (0.911)	43678.3	RC2_10.2	24346.1 (0.402)	24312.7 (0.264)	43850.54 (0.394)	43810.5 (0.303)	24248.6
RC1_10.3	42640.1 (1.230)	42554.8 (1.028)	42682.14 (1.330)	42622.4 (1.188)	42121.9	RC2_10.3	19711.2 (0.475)	19702.3 (0.429)	42293.37 (0.407)	42235.3 (0.269)	19618.1
RC1_10.4	41709.14 (0.850)	41636.4 (0.675)	41703.30 (0.836)	41644.8 (0.695)	41357.4	RC2_10.4	15818.48 (1.046)	15771.8 (0.748)	41797.16 (1.063)	41737.0 (0.918)	15654.7
RC1_10.5	45508.38 (1.067)	45310.1 (0.626)	45441.56 (0.918)	45395.9 (0.817)	45028.1	RC2_10.5	26030.96 (0.905)	25933.8 (0.528)	45375.23 (0.771)	45305.3 (0.616)	25797.5
RC1_10.6	45414.38 (1.150)	45285.5 (0.863)	45317.52 (0.934)	45192.3 (0.655)	44898.2	RC2_10.6	26082.16 (1.162)	25995.8 (0.827)	45441.04 (1.209)	45371.7 (1.055)	25782.5
RC1_10.7	44919.54 (1.150)	44859.5 (1.014)	44827.86 (0.943)	44738.8 (0.743)	44409	RC2_10.7	24586.98 (0.802)	24540.7 (0.612)	44796.62 (0.873)	44680.8 (0.612)	24391.4
RC1_10.8	44417.98 (1.142)	44360.2 (1.010)	44311.70 (0.900)	44267.1 (0.798)	43916.5	RC2_10.8	23558.98 (1.199)	23462.5 (0.785)	44358.84 (1.007)	44222.1 (0.696)	23279.8
RC1_10.9	44291.62 (0.989)	44225.9 (0.839)	44300.28 (1.008)	44215.9 (0.816)	43858	RC2_10.9	22932.06 (0.882)	22883.7 (0.669)	44300.52 (1.009)	44215.1 (0.814)	22731.6
RC1_10.10	43907.32 (0.858)	43854.3 (0.736)	43963.24 (0.987)	43884.5 (0.806)	43533.7	RC2_10.10	21992.64 (1.203)	21932.4 (0.926)	43982.60 (1.031)	43833.4 (0.688)	21731.2
Average Gap	0.916		0.801				0.766		0.698		
Median Gap	0.891		0.845				0.825		0.810		

References

- [1] Luca Accorsi, Andrea Lodi, and Daniele Vigo. “Guidelines for the computational testing of machine learning approaches to vehicle routing problems”. In: *Operations Research Letters* 50.2 (2022), pp. 229–234.
- [2] Luca Accorsi and Daniele Vigo. “A fast and scalable heuristic for the solution of large-scale capacitated vehicle routing problems”. In: *Transportation Science* 55.4 (2021), pp. 832–856.
- [3] Luca Accorsi and Daniele Vigo. “Routing one million customers in a handful of minutes”. In: *Computers & Operations Research* 164 (2024), p. 106562. ISSN: 0305-0548.
- [4] Asma M. Altabeeb, Abdulqader M. Mohsen, and Abdullatif Ghallab. “An improved hybrid firefly algorithm for capacitated vehicle routing problem”. In: *Applied Soft Computing* 84 (2019), p. 105728. ISSN: 1568-4946.
- [5] Florian Arnold, Michel Gendreau, and Kenneth Sörensen. “Efficiently solving very large-scale routing problems”. In: *Computers & Operations Research* 107 (2019), pp. 32–42. ISSN: 0305-0548.
- [6] Florian Arnold and Kenneth Sörensen. “Knowledge-guided local search for the vehicle routing problem”. In: *Computers & Operations Research* 105 (2019), pp. 32–46.
- [7] Florian Arnold et al. “PILS: exploring high-order neighborhoods by pattern mining and injection”. In: *Pattern Recognition* 116 (2021), p. 107957.
- [8] Emmanuel Bengio et al. “Flow network based generative models for non-iterative diverse candidate generation”. In: *Advances in neural information processing systems* 34 (2021), pp. 27381–27394.
- [9] Yoshua Bengio, Andrea Lodi, and Antoine Prouvost. “Machine learning for combinatorial optimization: a methodological tour d’horizon”. In: *European Journal of Operational Research* 290.2 (2021), pp. 405–421.
- [10] Yoshua Bengio et al. “Curriculum learning”. In: *Proceedings of the International Conference on Machine Learning*. Montreal, Quebec, Canada: Association for Computing Machinery, 2009, 41–48. ISBN: 9781605585161.
- [11] D.A. Beyer and R.G. Ogier. “Tabu learning: a neural network search method for solving nonconvex optimization problems”. In: *1991 International Joint Conference on Neural Networks (IJCNN)*. 1991, 953–961 vol.2.
- [12] Xavier Bresson and Thomas Laurent. *Residual Gated Graph ConvNets*. 2018. arXiv: 1711.07553 [cs.LG].
- [13] Xinyun Chen and Yuandong Tian. “Learning to Perform Local Rewriting for Combinatorial Optimization”. In: *Advances in Neural Information Processing Systems*. 2019.
- [14] Jan Christiaens and Greet Vanden Berghe. “Slack induction by string removals for vehicle routing problems”. In: *Transportation Science* 54.2 (2020), pp. 417–433.
- [15] Geoff Clarke and John W Wright. “Scheduling of vehicles from a central depot to a number of delivery points”. In: *Operations research* 12.4 (1964), pp. 568–581.
- [16] Paulo R d O da Costa et al. “Learning 2-opt Heuristics for the Traveling Salesman Problem via Deep Reinforcement Learning”. In: *Proceedings of The 12th Asian Conference on Machine Learning*. Vol. 129. Proceedings of Machine Learning Research. PMLR, 2020, pp. 465–480.
- [17] Janez Demšar. “Statistical Comparisons of Classifiers over Multiple Data Sets”. In: *Journal of Machine Learning Research* 7.1 (2006), pp. 1–30.
- [18] Marco Dorigo, Mauro Birattari, and Thomas Stutzle. “Ant colony optimization”. In: *IEEE Computational Intelligence Magazine* 1.4 (2006), pp. 28–39.

- [19] Vijay Prakash Dwivedi et al. “Benchmarking Graph Neural Networks”. In: *Journal of Machine Learning Research* 24.43 (2023), pp. 1–48.
- [20] Jonas K. Falkner et al. “Learning to Control Local Search for Combinatorial Optimization”. In: *Machine Learning and Knowledge Discovery in Databases*. Cham: Springer Nature Switzerland, 2023, pp. 361–376. ISBN: 978-3-031-26419-1.
- [21] Hermann Gehring and Jörg Homberger. “A parallel hybrid evolutionary metaheuristic for the vehicle routing problem with time windows”. In: *Proceedings of EUROGEN99*. Vol. 2. Citeseer, 1999, pp. 57–64.
- [22] Fred Glover. “Tabu search and adaptive memory programming—advances, applications and challenges”. In: *Interfaces in Computer Science and Operations Research: Advances in Metaheuristics, Optimization, and Stochastic Modeling Technologies* (1997).
- [23] Fred Glover and Manuel Laguna. “Tabu Search”. In: *Handbook of Combinatorial Optimization: Volume 1–3*. Boston, MA: Springer US, 1998, pp. 2093–2229. ISBN: 978-1-4613-0303-9.
- [24] M. Gori, G. Monfardini, and F. Scarselli. “A new model for learning in graph domains”. In: *Proceedings. 2005 IEEE International Joint Conference on Neural Networks, 2005*. Vol. 2. 2005, 729–734 vol. 2.
- [25] Chris Groër, Bruce Golden, and Edward Wasil. “A library of local search heuristics for the vehicle routing problem”. In: *Mathematical Programming Computation* 2 (2010), pp. 79–101.
- [26] Prateek Gupta et al. “Hybrid Models for Learning to Branch”. In: *Advances in Neural Information Processing Systems*. Vol. 33. Curran Associates, Inc., 2020, pp. 18087–18097.
- [27] Keld Helsgaun. “An extension of the Lin-Kernighan-Helsgaun TSP solver for constrained traveling salesman and vehicle routing problems”. In: *Roskilde: Roskilde University* 12 (2017).
- [28] John J Hopfield and David W Tank. ““Neural” computation of decisions in optimization problems”. In: *Biological cybernetics* 52.3 (1985), pp. 141–152.
- [29] André Hottung and Kevin Tierney. “Neural large neighborhood search for the capacitated vehicle routing problem”. In: *ECAI 2020*. IOS Press, 2020, pp. 443–450.
- [30] Benjamin Hudson et al. “Graph Neural Network Guided Local Search for the Traveling Salesperson Problem”. In: *International Conference on Learning Representations*. 2022.
- [31] Yuan Jiang et al. “Ensemble-based Deep Reinforcement Learning for Vehicle Routing Problems under Distribution Shift”. In: *Advances in Neural Information Processing Systems*. Vol. 36. 2023, pp. 53112–53125.
- [32] Chaitanya K Joshi, Thomas Laurent, and Xavier Bresson. “An efficient graph convolutional network technique for the travelling salesman problem”. In: *arXiv preprint arXiv:1906.01227* (2019).
- [33] Chaitanya K. Joshi et al. “Learning the travelling salesperson problem requires rethinking generalization”. In: *Constraints* 27.1–2 (Apr. 2022), 70–98. ISSN: 1572-9354.
- [34] Minsu Kim et al. “Ant Colony Sampling with GFlowNets for Combinatorial Optimization”. In: *The 28th International Conference on Artificial Intelligence and Statistics*. 2025.
- [35] Wouter Kool, Herke van Hoof, and Max Welling. “Attention, Learn to Solve Routing Problems!” In: *International Conference on Learning Representations*. 2019.
- [36] Wouter Kool et al. “Deep Policy Dynamic Programming for Vehicle Routing Problems”. In: *Integration of Constraint Programming, Artificial Intelligence, and Operations Research*. Cham: Springer International Publishing, 2022, pp. 190–213. ISBN: 978-3-031-08011-1.

- [37] Wouter Kool et al. “Hybrid genetic search for the vehicle routing problem with time windows: A high-performance implementation”. In: *12th DIMACS Implementation Challenge Workshop*. DIMACS, Rutgers University Piscataway, NJ. 2022.
- [38] Yeong-Dae Kwon et al. “POMO: Policy Optimization with Multiple Optima for Reinforcement Learning”. In: *Advances in Neural Information Processing Systems*. Vol. 33. 2020, pp. 21188–21198.
- [39] Gilbert Laporte. “Fifty years of vehicle routing”. In: *Transportation science* 43.4 (2009), pp. 408–416.
- [40] Sirui Li, Zhongxia Yan, and Cathy Wu. “Learning to delegate for large-scale vehicle routing”. In: *Advances in Neural Information Processing Systems* 34 (2021), pp. 26198–26211.
- [41] Yang Li et al. “T2T: From Distribution Learning in Training to Gradient Search in Testing for Combinatorial Optimization”. In: *Advances in Neural Information Processing Systems*. Vol. 36. 2023, pp. 50020–50040.
- [42] Hao Lu, Xingwen Zhang, and Shuang Yang. “A Learning-based Iterative Method for Solving Vehicle Routing Problems”. In: *International Conference on Learning Representations*. 2020.
- [43] Flavien Lucas, Romain Billot, and Marc Sevaux. “A comment on “what makes a VRP solution good? The generation of problem-specific knowledge for heuristics””. In: *Computers & Operations Research* 110 (2019), pp. 130–134.
- [44] Yining Ma, Zhiguang Cao, and Yeow Meng Chee. “Learning to Search Feasible and Infeasible Regions of Routing Problems with Flexible Neural k-Opt”. In: *Advances in Neural Information Processing Systems*. 2023.
- [45] Yining Ma et al. “Learning to iteratively solve routing problems with dual-aspect collaborative transformer”. In: *Advances in Neural Information Processing Systems* 34 (2021), pp. 11096–11107.
- [46] Yannis Marinakis. “An improved particle swarm optimization algorithm for the capacitated location routing problem and for the location routing problem with stochastic demands”. In: *Applied Soft Computing* 37 (2015), pp. 680–701. ISSN: 1568-4946.
- [47] Makoto Matsumoto and Takuji Nishimura. “Mersenne twister: a 623-dimensionally equidistributed uniform pseudo-random number generator”. In: *ACM Transactions on Modeling and Computer Simulation (TOMACS)* 8.1 (1998), pp. 3–30.
- [48] Juan Pablo Mesa et al. “Machine-learning component for multi-start metaheuristics to solve the capacitated vehicle routing problem”. In: *Applied Soft Computing* 173 (2025), p. 112916. ISSN: 1568-4946.
- [49] Mouad Morabit, Guy Desaulniers, and Andrea Lodi. “Machine-learning-based column selection for column generation”. In: *Transportation Science* 55.4 (2021), pp. 815–831.
- [50] Christopher Morris et al. “Weisfeiler and Leman Go Neural: Higher-Order Graph Neural Networks”. In: *Proceedings of the AAAI Conference on Artificial Intelligence*. 2019, pp. 4602–4609.
- [51] Harikrishna Narasimhan, Rohit Vaish, and Shivani Agarwal. “On the statistical consistency of plug-in classifiers for non-decomposable performance measures”. In: *Advances in neural information processing systems* 27 (2014).
- [52] Wenbin Ouyang et al. *Learning to Segment for Vehicle Routing Problems*. 2025. arXiv: 2507.01037 [cs.LG].
- [53] Christian Prins. “A simple and effective evolutionary algorithm for the vehicle routing problem”. In: *Computers & operations research* 31.12 (2004), pp. 1985–2002.

- [54] Caroline Prodhon and Christian Prins. “Metaheuristics for Vehicle Routing Problems”. In: *Metaheuristics*. Cham: Springer International Publishing, 2016, pp. 407–437.
- [55] Eduardo Queiroga et al. “10,000 optimal CVRP solutions for testing machine learning based heuristics”. In: *AAAI-22 Workshop on Machine Learning for Operations Research (ML4OR)* (2021).
- [56] Babak Rezaei et al. “Combining genetic local search into a multi-population Imperialist Competitive Algorithm for the Capacitated Vehicle Routing Problem”. In: *Applied Soft Computing* 142 (2023), p. 110309. ISSN: 1568-4946.
- [57] Franco Scarselli et al. “The Graph Neural Network Model”. In: *IEEE Transactions on Neural Networks* 20.1 (2009), pp. 61–80.
- [58] Shashank Singh and Justin T Khim. “Optimal binary classification beyond accuracy”. In: *Advances in Neural Information Processing Systems* 35 (2022), pp. 18226–18240.
- [59] Marius M. Solomon. “Algorithms for the Vehicle Routing and Scheduling Problems with Time Window Constraints”. In: *Operations Research* 35.2 (1987), pp. 254–265.
- [60] María Soto et al. “Multiple neighborhood search, tabu search and ejection chains for the multi-depot open vehicle routing problem”. In: *Computers & Industrial Engineering* 107 (2017), pp. 211–222.
- [61] Jingyan Sui et al. “Learning 3-opt heuristics for traveling salesman problem via deep reinforcement learning”. In: *Proceedings of The 13th Asian Conference on Machine Learning*. Vol. 157. Proceedings of Machine Learning Research. PMLR, 2021, pp. 1301–1316.
- [62] Nasrin Sultana et al. “Learning to guide local search optimisation for routing problems”. In: *Operations Research Letters* 55 (2024), p. 107136. ISSN: 0167-6377.
- [63] Paolo Toth and Daniele Vigo. *Vehicle routing: problems, methods, and applications*. SIAM, 2014.
- [64] Petar Veličković et al. “Graph Attention Networks”. In: *International Conference on Learning Representations*. 2018.
- [65] Thibaut Vidal. “Hybrid genetic search for the CVRP: Open-source implementation and SWAP* neighborhood”. In: *Computers & Operations Research* 140 (2022), p. 105643.
- [66] Yaoxin Wu et al. “Learning improvement heuristics for solving routing problems”. In: *IEEE transactions on neural networks and learning systems* 33.9 (2021), pp. 5057–5069.
- [67] Liang Xin et al. “Multi-decoder attention model with embedding glimpse for solving vehicle routing problems”. In: *Proceedings of the AAAI Conference on Artificial Intelligence*. 2021, pp. 12042–12049.
- [68] Liang Xin et al. “NeuroLKH: Combining deep learning model with lin-kernighan-helsgaun heuristic for solving the traveling salesman problem”. In: *Advances in Neural Information Processing Systems* 34 (2021), pp. 7472–7483.
- [69] Senyan Yang et al. “Adaptive large neighborhood search incorporating mixed-integer linear programming for electric vehicle routing problem with mobile charging and nonlinear battery degradation”. In: *Applied Soft Computing* 175 (2025), p. 112988. ISSN: 1568-4946.
- [70] Haoran Ye et al. “DeepACO: Neural-enhanced Ant Systems for Combinatorial Optimization”. In: *Advances in Neural Information Processing Systems*. 2023.
- [71] José Eduardo Zárate-Aranda and José C. Ortiz-Bayliss. “Machine-learning-based hyper-heuristics for solving the Knapsack Problem”. In: *Pattern Recognition Letters* (2025). ISSN: 0167-8655.